

# Quantifying the nitrogen isotope effects during photochemical equilibrium between NO and NO<sub>2</sub>: implications for δ<sup>15</sup>N in tropospheric reactive nitrogen

Jianghanyang Li<sup>1</sup>, Xuan Zhang<sup>2</sup>, John Orlando<sup>2</sup>, Geoffrey Tyndall<sup>2</sup> and Greg Michalski<sup>1,3</sup>

<sup>1</sup> Department of Earth, Atmospheric and Planetary Sciences, Purdue University, West Lafayette, IN, 47907

<sup>2</sup> Atmospheric Chemistry Observations and Modeling Lab, National Center for Atmospheric Research, Boulder, CO, 80301

<sup>3</sup> Department of Chemistry, Purdue University, West Lafayette, IN, 47907

*Correspondence to:* Jianghanyang Li (li2502@purdue.edu)

**Abstract.** Nitrogen isotope fractionations between nitrogen oxides (NO and NO<sub>2</sub>) play a significant role in determining the nitrogen isotopic compositions (δ<sup>15</sup>N) of atmospheric reactive nitrogen. Both the equilibrium isotopic exchange between NO and NO<sub>2</sub> molecules and the isotope effects occurring during the NO<sub>x</sub> photochemical cycle are important, but both are not well constrained. The nighttime and daytime isotopic fractionations between NO and NO<sub>2</sub> in an atmospheric simulation chamber at atmospherically relevant NO<sub>x</sub> levels were measured. Then, the impact of NO<sub>x</sub> level and NO<sub>2</sub> photolysis rate to the combined isotopic fractionation (equilibrium isotopic exchange and photochemical cycle) between NO and NO<sub>2</sub> were calculated. It was found that the isotope effects occurring during the NO<sub>x</sub> photochemical cycle can be described using a single fractionation factor, designated the Leighton Cycle Isotope Effect (LCIE). The results showed that at room temperature, the fractionation factor of nitrogen isotopic exchange is 1.0289±0.0019, and the fractionation factor of LCIE (when O<sub>3</sub> solely controls the oxidation from NO to NO<sub>2</sub>) is 0.990±0.005. The measured LCIE factor showed good agreement with previous field measurements, suggesting that it could be applied in ambient environment, although future work is needed to assess the isotopic fractionation factors of NO + RO<sub>2</sub>/HO<sub>2</sub> → NO<sub>2</sub>. The results were used to model the NO-NO<sub>2</sub> isotopic fractionations under several NO<sub>x</sub> conditions. The model suggested that isotopic exchange was the dominate factor when NO<sub>x</sub> >20 nmol mol<sup>-1</sup>, while LCIE was more important at low NO<sub>x</sub> concentrations (<1 nmol mol<sup>-1</sup>) and high rates of NO<sub>2</sub> photolysis. These findings provided a useful tool to quantify the isotopic fractionations between tropospheric NO and NO<sub>2</sub>, which can be applied in future field observations and atmospheric chemistry models.

## 33 1. Introduction

34 The nitrogen isotopic composition ( $\delta^{15}\text{N}$ ) of reactive nitrogen compounds in the  
35 atmosphere is an important tool in understanding the sources and chemistry of atmospheric  $\text{NO}_x$   
36 ( $\text{NO}+\text{NO}_2$ ). It has been suggested that the  $\delta^{15}\text{N}$  value of atmospheric nitrate ( $\text{HNO}_3$ , nitrate  
37 aerosols and nitrate ions in the precipitation and snow) imprints the  $\delta^{15}\text{N}$  value of  $\text{NO}_x$  sources  
38 (Elliott et al., 2009; Kendall et al., 2007) thus many studies have used the  $\delta^{15}\text{N}$  values of  
39 atmospheric nitrate to investigate  $\text{NO}_x$  sources (Chang et al., 2018; Felix et al., 2012; Felix &  
40 Elliott, 2014; Gobel et al., 2013; Hastings et al., 2004, 2009; Morin et al., 2009; Park et al., 2018;  
41 Walters et al., 2015, 2018). However, there remain questions about how isotopic fractionations  
42 that may occur during photochemical cycling of  $\text{NO}_x$  could alter the  $\delta^{15}\text{N}$  values as it partitions  
43 into  $\text{NO}_y$  ( $\text{NO}_y$  = atmospheric nitrate,  $\text{NO}_3$ ,  $\text{N}_2\text{O}_5$ ,  $\text{HONO}$ , etc., Chang et al., 2018; Freyer, 1991;  
44 Hastings et al., 2004; Jarvis et al., 2008; Michalski et al., 2005; Morin et al., 2009; Zong et al.,  
45 2017). Similarly, other complex reactive nitrogen chemistry, such as nitrate photolysis and re-  
46 deposition in ice and snow (Frey et al., 2009), may impact the  $\delta^{15}\text{N}$  of  $\text{NO}_y$  and atmospheric nitrate.  
47 The fractionation between  $\text{NO}$  and  $\text{NO}_2$  via isotope exchange has been suggested to be the  
48 dominant factor in determining the  $\delta^{15}\text{N}$  of  $\text{NO}_2$  and ultimately atmospheric nitrate (Freyer, 1991;  
49 Freyer et al., 1993; Savarino et al., 2013; Walters et al., 2016). However, isotopic fractionations  
50 occur in most, if not all,  $\text{NO}_x$  and  $\text{NO}_y$  reactions, while most of these are still unknown or, if  
51 calculated (Walters and Michalski, 2015), unverified by experiments. Since the atmospheric  
52 chemistry of  $\text{NO}_y$  varies significantly in different environments (e.g., polluted vs. pristine, night  
53 vs. day), the isotopic fractionations associated with  $\text{NO}_y$  chemistry are also likely to vary in  
54 different environments. These unknowns could potentially bias conclusions about  $\text{NO}_x$  source  
55 apportionment reached when using nitrogen isotopes. Therefore, understanding the isotopic

56 fractionations between NO and NO<sub>2</sub> during photochemical cycling could improve our  
57 understanding of the relative role of sources versus chemistry for controlling the δ<sup>15</sup>N variations  
58 of atmospheric NO<sub>2</sub> and nitrate.

59 In general, there are three types of isotopic fractionation effects associated with NO<sub>x</sub>  
60 chemistry (Fig. 1A). The first type is the equilibrium isotopic effect (EIE), i.e., isotope exchange  
61 between two compounds without forming new molecules (Urey, 1947, Bigeleisen and Mayer,  
62 1947), which for nitrogen isotopes in the NO<sub>x</sub> system is the  $^{15}\text{NO} + ^{14}\text{NO}_2 \leftrightarrow ^{14}\text{NO} + ^{15}\text{NO}_2$   
63 exchange reaction (Begun and Melton, 1956, Walters et al., 2016). The second type is the kinetic  
64 isotopic effect (KIE) associated with difference in isotopologue rate coefficients during  
65 unidirectional reactions (Bigeleisen & Wolfsberg, 1957). In the NO<sub>x</sub> system this KIE would  
66 manifest in the oxidation of NO into NO<sub>2</sub> by O<sub>3</sub>/HO<sub>2</sub>/RO<sub>2</sub>. The third type is the photochemical  
67 isotope fractionation effect (PHIFE, Miller & Yung, 2000), which for NO<sub>x</sub> is the isotopic  
68 fractionation associated with NO<sub>2</sub> photolysis. All three fractionations could impact the δ<sup>15</sup>N value  
69 of NO<sub>2</sub>, and consequently atmospheric nitrate, but the relative importance of each may vary.

70 The limited number of studies on the EIE in the NO<sub>x</sub> cycle have significant uncertainties.  
71 Discrepancies in the EIE for  $^{15}\text{NO} + ^{14}\text{NO}_2 \leftrightarrow ^{14}\text{NO} + ^{15}\text{NO}_2$  have been noted in several studies.  
72 Theoretical calculations predicted isotope fractionation factors (α) ranging from 1.035 to 1.042 at  
73 room temperature (Begun & Fletcher, 1960; Monse et al., 1969; Walters & Michalski, 2015) due  
74 to the different approximations used to calculate harmonic frequencies in each study. Likewise,  
75 two separate experiments measured different room temperature fractionation factors of  
76  $1.028 \pm 0.002$  (Begun & Melton, 1956) and  $1.0356 \pm 0.0015$  (Walters et al., 2016). A concern in both  
77 experiments is that they were conducted in small chambers with high NO<sub>x</sub> concentrations  
78 (hundreds of μmol mol<sup>-1</sup>), significantly higher than typical ambient atmospheric NO<sub>x</sub> levels

79 (usually less than  $0.1 \mu\text{mol mol}^{-1}$ ). Whether the isotopic fractionation factors determined by these  
80 experiments are applicable in the ambient environment is uncertain because of possible wall effects  
81 and formation of higher oxides, notably  $\text{N}_2\text{O}_4$  and  $\text{N}_2\text{O}_3$  at these high  $\text{NO}_x$  concentrations.

82 Even less research has examined the KIE and PHIFE occurring during  $\text{NO}_x$  cycling. The  
83 KIE of  $\text{NO} + \text{O}_3$  has been theoretically calculated (Walters and Michalski, 2016) but has not been  
84 experimentally verified. The  $\text{NO}_2$  PHIFE has not been experimentally determined or theoretically  
85 calculated. As a result, field observation studies often overlook the effects of PHIFE and KIE.  
86 Freyer et al. (1993) measured  $\text{NO}_x$  concentrations and the  $\delta^{15}\text{N}$  values of  $\text{NO}_2$  over a 1-year period  
87 at Jülich, Germany and inferred a combined  $\text{NO}_x$  isotope fractionation factor (EIE+KIE+PHIFE)  
88 of  $1.018 \pm 0.001$ . Freyer et al. (1993) suggested that the  $\text{NO}_x$  photochemical cycle (KIE and PHIFE)  
89 tends to diminish the equilibrium isotopic fractionation (EIE) between  $\text{NO}$  and  $\text{NO}_2$ . Even if this  
90 approach were valid, applying this single fractionation factor elsewhere, where  $\text{NO}_x$ ,  $\text{O}_3$   
91 concentrations and actinic fluxes are different, would be tenuous given that these factors may  
92 influence the relative importance of EIE, KIE and PHIFE (Hastings et al., 2004; Walters et al.,  
93 2016). Therefore, to quantify the overall isotopic fractionations between  $\text{NO}$  and  $\text{NO}_2$  at various  
94 tropospheric conditions, it is crucial to know 1) isotopic fractionation factors of EIE, KIE and  
95 PHIFE individually and 2) the relative importance of each factor under various conditions.

96 In this work, we aim to quantify the nitrogen isotope fractionation factors between  $\text{NO}$  and  
97  $\text{NO}_2$  at photochemical equilibrium. First, we measure the N isotope fractionations between  $\text{NO}$   
98 and  $\text{NO}_2$  in an atmospheric simulation chamber at atmospherically relevant  $\text{NO}_x$  levels. Then, we  
99 provide mathematical solutions to assess the impact of  $\text{NO}_x$  level and  $\text{NO}_2$  photolysis rate ( $j(\text{NO}_2)$ )  
100 to the relative importance of EIE, KIE and PHIFE. Subsequently we use the solutions and chamber  
101 measurements to calculate the isotopic fractionation factors of EIE, KIE and PHIFE. Lastly, using

102 the calculated fractionation factors and the equations, we model the NO-NO<sub>2</sub> isotopic  
103 fractionations at several sites to illustrate the behavior of  $\delta^{15}\text{N}$  values of NO<sub>x</sub> in the ambient  
104 environment.

105

## 106 **2. Methods**

107 The experiments were conducted using a 10 m<sup>3</sup> Atmospheric Simulation Chamber at the  
108 National Center for Atmospheric Research (see descriptions in Appendix A and Zhang et al.  
109 (2018)). A set of mass flow controllers was used to inject NO and O<sub>3</sub> into the chamber. NO was  
110 injected at 1 L min<sup>-1</sup> from an in-house NO/N<sub>2</sub> cylinder (133.16  $\mu\text{mol mol}^{-1}$  NO in ultra-pure N<sub>2</sub>),  
111 and O<sub>3</sub> was generated by flowing 5 L min<sup>-1</sup> zero-air through a flow tube equipped with a UV Pen-  
112 Ray lamp (UVP LLC., CA) into the chamber. NO and NO<sub>2</sub> concentrations were monitored in real  
113 time by chemiluminescence with a detection limit of 0.5 nmol mol<sup>-1</sup> (model CLD 88Y, Eco Physics,  
114 MI) as were O<sub>3</sub> concentrations using an UV absorption spectroscopy with a detection limit of 0.5  
115 nmol mol<sup>-1</sup> (model 49, Thermo Scientific, CO). In each experiment, the actual amounts of NO and  
116 O<sub>3</sub> injected were calculated using measured NO<sub>x</sub> and O<sub>3</sub> concentrations after steady state was  
117 reached (usually within 1 h). The wall loss rate of NO<sub>2</sub> was tested by monitoring O<sub>3</sub> (29 nmol mol<sup>-1</sup>  
118 <sup>1</sup>) and NO<sub>x</sub> (62 nmol mol<sup>-1</sup>) over a 4-hour period. After the NO and NO<sub>2</sub> concentrations reached  
119 steady state, no decrease in NO<sub>2</sub> concentrations was observed showing that chamber wall loss was  
120 negligible.

121 Three experiments were conducted to measure the  $\delta^{15}\text{N}$  value of the tank NO (i.e., the  $\delta^{15}\text{N}$   
122 value of total NO<sub>x</sub>). In each of these experiments, a certain amount of O<sub>3</sub> was first injected into the  
123 chamber, then approximately the same amount of NO was injected into the chamber to ensure 100%  
124 of the NO<sub>x</sub> was in the form of NO<sub>2</sub> with little O<sub>3</sub> (<15 nmol mol<sup>-1</sup>) remaining in the chamber, such

125 that the  $O_3+NO_2$  reaction was negligible. The  $NO_2$  in the chamber was then collected and its  $\delta^{15}N$   
126 value measured, which equates to the  $\delta^{15}N$  value of the tank NO.

127 Two sets of experiments were conducted to separately investigate the EIE, KIE and PHIFE.  
128 The first set of experiments was conducted in the dark. In each of these dark experiments, a range  
129 of NO and  $O_3$  ( $[O_3]<[NO]$ ) was injected into the chamber to produce NO- $NO_2$  mixtures with  
130  $[NO]/[NO_2]$  ratios ranging from 0.43 to 1.17. The N isotopes of these mixtures were used to  
131 investigate the EIE between NO and  $NO_2$ . The second set of experiments was conducted under  
132 irradiation of UV lights (300-500 nm, see Appendix A for irradiation spectrum). Under such  
133 conditions, NO,  $NO_2$  and  $O_3$  reached photochemical steady state, which combined the isotopic  
134 effects of EIE, KIE and PHIFE.

135 In all experiments, the concentrations of NO,  $NO_2$  and  $O_3$  were allowed to reach steady  
136 state, and the product  $NO_2$  was collected from the chamber using a honeycomb denuder tube. After  
137 the NO,  $NO_2$  and  $O_3$  concentrations reached steady-state, well-mixed chamber air was drawn out  
138 through a 40 cm long Norprene Thermoplastic tubing at  $10\text{ L min}^{-1}$  and passed through a  
139 honeycomb denuder system (Chemcomb 3500, Thermo Scientific). Based on flow rate, the  $NO_2$   
140 residence time in the was less than 0.5 second, thus in the light-on experiments where NO and  $O_3$   
141 coexisted, the  $NO_2$  produced inside the transfer tube through  $NO+O_3$  reactions should be  $<0.03$   
142  $\text{nmol mol}^{-1}$  (using the upper limit of NO and  $O_3$  concentrations in our experiments). The  
143 honeycomb denuder system consisted of two honeycomb denuder tubes connected in series. Each  
144 honeycomb denuder tube is a glass cylinder of 38 mm long, 47 mm in diameter, and consist of 212  
145 hexagonal tubes with inner diameters of 2 mm. Before collecting samples, each denuder tube was  
146 coated with a solution of 10% KOH and 25% guaiacol in methanol and then dried by flowing  $N_2$   
147 gas through the denuder tube for 15 seconds (Williams and Grosjean, 1990, Walters et al., 2016).

148 The  $\text{NO}_2$  reacted with guaiacol coating and was converted into  $\text{NO}_2^-$  that was retained on the  
149 denuder tube wall (Williams and Grosjean, 1990). NO was inert to the denuder tube coating: a  
150 control experiment sampled pure NO using the denuder tubes, which did not show any measurable  
151  $\text{NO}_2^-$ . The  $\text{NO}_2$  collection efficiency of a single honeycomb denuder tube was tested in another  
152 control experiment: air containing  $66 \text{ nmol mol}^{-1}$  of  $\text{NO}_2$  was drawn out of the chamber through a  
153 denuder tube, and the  $\text{NO}_2$  concentration at the exit of the tube holder was measured and found to  
154 be below the detection limit ( $<1 \text{ nmol mol}^{-1}$ ), suggesting the collection efficiency was nearly 100%  
155 when  $[\text{NO}_2] < 66 \text{ nmol mol}^{-1}$ . Furthermore, when the denuder system consisted of two denuder  
156 tubes in series and  $\text{NO}_2^-$  in the second denuder was below the detection limit indicating trivial  $\text{NO}_2$   
157 breakthrough. Each  $\text{NO}_2$  collection lasted for 0.5-3 hours in order to collect enough  $\text{NO}_2^-$  for  
158 isotopic analysis (at least 300 nmol). After collection, the  $\text{NO}_2^-$  was leached from each denuder  
159 tube by rinsing thoroughly with 10 ml deionized water into a clean polypropylene container and  
160 stored frozen until isotopic analysis. Isotopic analysis was conducted at Purdue Stable Isotope  
161 Laboratory. For each sample, approximately 50 nmol of the  $\text{NO}_2^-$  extract was mixed with 2 M  
162 sodium azide solution in acetic acid buffer in an air-tight glass vial, then shaken overnight to  
163 completely reduce all the  $\text{NO}_2^-$  to  $\text{N}_2\text{O}_{(\text{g})}$  (Casciotti & McIlvin, 2007; McIlvin & Altabet, 2005).  
164 The product  $\text{N}_2\text{O}$  was directed into a Thermo GasBench equipped with cryo-trap, then the  $\delta^{15}\text{N}$  of  
165 the  $\text{N}_2\text{O}$  was measured using a Delta-V Isotope Ratios Mass Spectrometer. Six coated denuders  
166 tubes that did not get exposed to  $\text{NO}_2$  were also analyzed using the same chemical procedure,  
167 which did not show any measurable signal on the IRMS, suggesting the blank from both sampling  
168 process and the chemical conversion process was negligible. The overall analytical uncertainty for  
169  $\delta^{15}\text{N}$  analysis was 0.5 ‰ ( $1\sigma$ ) based on replicate analysis of in house  $\text{NO}_2^-$  standards.

170

### 171 3. Results and Discussions

#### 172 3.1. Equilibrium Isotopic Fractionation between NO and NO<sub>2</sub>

173 The equilibrium isotope fractionation factor,  $\alpha(\text{NO}_2\text{-NO})$ , is the <sup>15</sup>N enrichment in NO<sub>2</sub>  
174 relative to NO, and is expressed as the ratio of rate constants  $k_2 / k_1$  of two reactions:



177 where  $k_1$  is the rate constant of the isotopic exchange, which was previously determined to be  
178  $8.14 \times 10^{-14} \text{ cm}^3 \text{ s}^{-1}$  (Sharma et al., 1970). The reaction time required for NO-NO<sub>2</sub> to reach isotopic  
179 equilibrium was estimated using the exchange rate constants in a simple kinetics box model  
180 (BOXMOX, Knotte et al., 2015). The model predicts that at typical NO<sub>x</sub> concentrations used during  
181 the chamber experiments (7.7-62.4 nmol mol<sup>-1</sup>), isotopic equilibrium would be reached within 15  
182 minutes (see Appendix B). Since the sample collection usually started 1 hour after NO<sub>x</sub> was well  
183 mixed in the chamber, there was sufficient time to reach full isotope equilibrium. The isotope  
184 equilibrium fractionation factor ( $\alpha(\text{NO}_2\text{-NO})$ ) is then calculated to be:

185 
$$\alpha(\text{NO}_2 - \text{NO}) = \frac{[^{15}\text{NO}_2][^{14}\text{NO}]}{[^{14}\text{NO}_2][^{15}\text{NO}]} = \frac{R(\text{NO}_2)}{R(\text{NO})}$$
 Eq. (1)

186 where  $R(\text{NO}, \text{NO}_2)$  are the <sup>15</sup>N/<sup>14</sup>N ratios of NO and NO<sub>2</sub>. By definition, the  
187  $\delta^{15}\text{N}(\text{NO}) = (R(\text{NO})/R(\text{reference}) - 1) \times 1000 \text{ ‰}$  and  $\delta^{15}\text{N}(\text{NO}_2) = (R(\text{NO}_2)/R(\text{reference}) - 1) \times 1000 \text{ ‰}$ ,  
188 but hereafter, the  $\delta^{15}\text{N}$  values of NO, NO<sub>2</sub> and NO<sub>x</sub> will be referred as  $\delta(\text{NO})$ ,  $\delta(\text{NO}_2)$  and  $\delta(\text{NO}_x)$ ,  
189 respectively. Eq. (1) leads to:

190 
$$\delta(\text{NO}_2) - \delta(\text{NO}) = (\alpha(\text{NO}_2 - \text{NO}) - 1) (1 + \delta(\text{NO}))$$
 Eq. (2)

191 Using Eq. (2) and applying NO<sub>x</sub> isotopic mass balance ( $\delta(\text{NO}_x) = f(\text{NO}_2)\delta(\text{NO}_2) + (1 - f(\text{NO}_2))\delta(\text{NO})$ ),  
192  $f(\text{NO}_2) = [\text{NO}_2] / ([\text{NO}] + [\text{NO}_2])$ ) yields:

193 
$$\frac{\delta(\text{NO}_2) - \delta(\text{NO}_x)}{1 + \delta(\text{NO}_2)} = \frac{\alpha(\text{NO}_2 - \text{NO}) - 1}{\alpha(\text{NO}_2 - \text{NO})} (1 - f(\text{NO}_2))$$
 Eq. (3)



194 Here,  $\delta(\text{NO}_x)$  equals to the  $\delta^{15}\text{N}$  value of the cylinder NO and  $f(\text{NO}_2)$  is the molar fraction of  $\text{NO}_2$   
195 with respect to total  $\text{NO}_x$ . Three experiments (Table 1) that measured  $\delta(\text{NO}_x)$  showed consistent  
196  $\delta(\text{NO}_x)$  values of  $(-58.7 \pm 0.8) \text{‰}$  ( $n = 3$ ), indicating  $\delta(\text{NO}_x)$  remained unchanged throughout the  
197 experiments (as expected for isotope mass balance). Thus, the  $\delta(\text{NO}_x)$  can be treated as a constant  
198 in Eq. (3), and the linear regression of  $(\delta(\text{NO}_2) - \delta(\text{NO}_x)) / (1 + \delta(\text{NO}_2))$  versus  $1 - f(\text{NO}_2)$  should have  
199 an intercept of 0 and a slope of  $(\alpha(\text{NO}_2\text{-NO}) - 1) / \alpha(\text{NO}_2\text{-NO})$ .

200 The plot of  $(\delta(\text{NO}_2) - \delta(\text{NO}_x)) / (1 + \delta(\text{NO}_2))$  as a function of  $1 - f(\text{NO}_2)$  values from five  
201 experiments yields an  $\alpha(\text{NO}_2\text{-NO})$  value of  $1.0289 \pm 0.0019$  at room temperature (Fig. 1B and Table  
202 1). This fractionation factor is comparable to previously measured values but with some  
203 differences. Our result agrees well with the  $\alpha(\text{NO}_2\text{-NO})$  value of  $1.028 \pm 0.002$  obtained by Begun  
204 and Melton (1956) at room temperature. However, Walters et al., (2016) determined the  $\alpha(\text{NO}_2\text{-}$   
205  $\text{NO})$  values of  $\text{NO-NO}_2$  exchange in a 1-liter reaction vessel, which showed a slightly higher  
206  $\alpha(\text{NO}_2\text{-NO})$  value of 1.035. This discrepancy might originate from rapid heterogeneous reactions  
207 on the wall of the reaction vessel at high  $\text{NO}_x$  concentrations and the small chamber size used by  
208 Walters et al. (2016). They used a reaction vessel made of Pyrex, which is known to absorb water  
209 (Do Remus et al., 1983; Takei et al., 1997) that can react with  $\text{NO}_2$  forming HONO,  $\text{HNO}_3$  and  
210 other N compounds. Additionally, previous studies have suggested that Pyrex walls enhance the  
211 formation rate of  $\text{N}_2\text{O}_4$  by over an order of magnitude (Barney & Finlayson-Pitts, 2000; Saliba et  
212 al., 2001), which at isotopic equilibrium is enriched in  $^{15}\text{N}$  compared to NO and  $\text{NO}_2$  (Walters &  
213 Michalski, 2015). Therefore, their measured  $\alpha(\text{NO}_2\text{-NO})$  might be slightly higher than the actual  
214  $\alpha(\text{NO}_2\text{-NO})$  value. In this work, the  $10 \text{ m}^3$  chamber has a much smaller surface to volume ratio  
215 relative to Walters et al. (2016) which minimizes wall effects, and the walls were made of Teflon  
216 that minimize  $\text{NO}_2$  surface reactivity, which was evidenced by the  $\text{NO}_2$  wall loss control

217 experiment. Furthermore, the low NO<sub>x</sub> mixing ratios in our experiments minimized N<sub>2</sub>O<sub>4</sub> and N<sub>2</sub>O<sub>3</sub>  
218 formation. At NO and NO<sub>2</sub> concentrations of 50 nmol mol<sup>-1</sup> the steady state concentrations of N<sub>2</sub>O<sub>4</sub>  
219 and N<sub>2</sub>O<sub>3</sub> were calculated to be 0.014 and 0.001 pmol mol<sup>-1</sup>, respectively (Atkinson et al., 2004).  
220 Therefore, we suggest our measured  $\alpha(\text{NO}_2\text{-NO})$  value (1.0289±0.0019) may better reflect the  
221 room temperature (298 K) NO-NO<sub>2</sub> EIE in the ambient environment.

222         Unfortunately, the chamber temperature could not be controlled so we were not able to  
223 investigate the temperature dependence of the EIE. Hence, we speculate that the  $\alpha(\text{NO}_2\text{-NO})$   
224 follows a similar temperature dependence pattern calculated in Walters et al. (2016). Walters et al.  
225 (2016) suggested that, the  $\alpha(\text{NO}_2\text{-NO})$  value would be 0.0047 higher at 273 K and 0.002 lower at  
226 310 K, relative to room temperature (298 K). Using this pattern and our experimentally determined  
227 data, we suggest the  $\alpha(\text{NO}_2\text{-NO})$  values at 273 K, 298 K and 310 K are 1.0336±0.0019,  
228 1.0289±0.0019 and 1.0269±0.0019, respectively. This 0.0067 variation at least partially contribute  
229 to the daily and seasonal variations of  $\delta^{15}\text{N}$  values of NO<sub>2</sub> and nitrate in some areas (e.g., polar  
230 regions with strong seasonal temperature variation). Thus, future investigations should be  
231 conducted to verify the EIE temperature dependence.

232

### 233 **3.2. Kinetic isotopic fractionation of Leighton Cycle**

234         The photochemical reactions of NO<sub>x</sub> will compete with the isotope exchange fractionations  
235 between NO and NO<sub>2</sub>. The NO-NO<sub>2</sub> photochemical cycle in the chamber was controlled by the  
236 Leighton cycle: NO<sub>2</sub> photolysis and the NO + O<sub>3</sub> reaction. This is because there were no VOCs in  
237 the chamber so no RO<sub>2</sub> was produced, which excludes the NO + RO<sub>2</sub> reaction. Likewise, the low  
238 water vapor content (RH<10%) and the minor flux of photons < 310 nm results in minimal OH  
239 production and hence little HO<sub>2</sub> formation and subsequently trivial amount of NO<sub>2</sub> would be

240 formed by NO + HO<sub>2</sub>. Applying these limiting assumptions, the EIE between NO and NO<sub>2</sub> (R1-  
 241 R2) were only competing with the KIE (R3-R4) and the PHIFE in R5-R6:



246 In which  $j(\text{NO}_2)$  is the NO<sub>2</sub> photolysis rate ( $1.4 \times 10^{-3} \text{ s}^{-1}$  in these experiments),  $k_5$  is the rate constant  
 247 for the NO+O<sub>3</sub> reaction ( $1.73 \times 10^{-14} \text{ cm}^3 \text{ s}^{-1}$ , Atkinson et al., 2004), and  $\alpha_{1,2}$  are isotopic  
 248 fractionation factors for the two reactions. Previous studies (Freyer et al., 1993; Walters et al.,  
 249 2016) have attempted to assess the competition between EIE (R1-R2), KIE and PHIFE (R3-R6),  
 250 but none of them quantified the relative importance of the two processes, nor were  $\alpha_1$  or  $\alpha_2$  values  
 251 experimentally determined. Here we provide the mathematical solution of EIE, KIE and PHIFE to  
 252 illustrate how R1-R6 affect the isotopic fractionations between NO and NO<sub>2</sub>.

253 First, the NO<sub>2</sub> lifetime with respect to isotopic exchange with NO ( $\tau_{\text{exchange}}$ ) and photolysis  
 254 ( $\tau_{\text{photo}}$ ) was determined:

255 
$$\tau_{\text{exchange}} = \frac{1}{k_1 [\text{NO}]}$$
 Eq. (4)

256 
$$\tau_{\text{photo}} = \frac{1}{j(\text{NO}_2)}$$
 Eq. (5)

257 We then define an A factor:

258 
$$A = \begin{cases} \frac{\tau_{\text{exchange}}}{\tau_{\text{photo}}} & \text{when } j(\text{NO}_2) \neq 0 \\ 0 & \text{when } j(\text{NO}_2) = 0 \end{cases}$$
 Eq. (6)

259 Using R1-R6 and Eq. (1)-(6), we solved steady-state  $\delta(\text{NO}_2)$  and  $\delta(\text{NO})$  values (see calculations  
 260 in Appendix C). Our calculations show that the  $\delta(\text{NO}_2)$ - $\delta(\text{NO})$  and  $\delta(\text{NO}_2)$ - $\delta(\text{NO}_x)$  values at steady  
 261 state can be expressed as functions of  $\alpha_1$ ,  $\alpha_2$ ,  $\alpha(\text{NO}_2\text{-NO})$  and A:

$$262 \quad \delta(\text{NO}_2) - \delta(\text{NO}) = \frac{(\alpha_2 - \alpha_1) A + (\alpha(\text{NO}_2\text{-NO}) - 1)}{\alpha_2 A + \alpha(\text{NO}_2\text{-NO})} (1 + \delta(\text{NO}_2))$$

$$263 \quad \approx \frac{(\alpha_2 - \alpha_1) A + (\alpha(\text{NO}_2\text{-NO}) - 1)}{A + 1} (1 + \delta(\text{NO}_2)) \quad \text{Eq. (7)}$$

$$264 \quad \delta(\text{NO}_2) - \delta(\text{NO}_x) = \frac{(\alpha_2 - \alpha_1) A + (\alpha(\text{NO}_2\text{-NO}) - 1)}{\alpha_2 A + \alpha(\text{NO}_2\text{-NO})} (1 + \delta(\text{NO}_2))(1 - f(\text{NO}_2))$$

$$265 \quad \approx \frac{(\alpha_2 - \alpha_1) A + (\alpha(\text{NO}_2\text{-NO}) - 1)}{A + 1} (1 + \delta(\text{NO}_2))(1 - f(\text{NO}_2)) \quad \text{Eq. (8)}$$

266 Equation (7) shows the isotopic fractionation between NO and NO<sub>2</sub> ( $\delta(\text{NO}_2)$ - $\delta(\text{NO})$ ) is mainly  
 267 determined by A, the EIE factor ( $\alpha(\text{NO}_2\text{-NO})-1$ ) and the  $(\alpha_2-\alpha_1)$  factor assuming  $(1+\delta(\text{NO}_2))$  is  
 268 close to 1. This  $(\alpha_2-\alpha_1)$  represents a combination of KIE and PHIFE, suggesting they act together  
 269 as one factor; therefore, we name the  $(\alpha_2-\alpha_1)$  factor Leighton Cycle Isotopic Effect, i.e., LCIE.  
 270 Using measured  $\delta(\text{NO}_2)$ ,  $\delta(\text{NO}_x)$  values, A values (Table 1), and the previously determined  $\alpha(\text{NO}_2\text{-}$   
 271 NO) value, We plot  $\frac{\delta(\text{NO}_2) - \delta(\text{NO}_x)}{(1 + \delta(\text{NO}_2))(1 - f(\text{NO}_2))}$  (equals to  $\frac{\delta(\text{NO}_2) - \delta(\text{NO})}{(1 + \delta(\text{NO}_2))}$ ) against A value and use Equations  
 272 (7) and (8) to estimate the  $(\alpha_2-\alpha_1)$  value (Fig. 1C). The plot shows that the best fit for the LCIE  
 273 factor is  $(-10 \pm 5)$  ‰ (Rooted Mean Square Error, RMSE, was lowest when  $\alpha_2-\alpha_1 = -10\%$ ). The  
 274 uncertainties in the LCIE factor are relatively higher than that of the EIE factor, mainly because  
 275 of the accumulated analytical uncertainties at low NO<sub>x</sub> and O<sub>3</sub> concentrations, and low A values  
 276 (0.10-0.28) due to the relatively low  $j(\text{NO}_2)$  value ( $1.4 \times 10^{-3} \text{ s}^{-1}$ ) under the chamber irradiation  
 277 conditions.

278 This LCIE factor determined in our experiments is in good agreement with theoretical  
 279 calculations. Walters and Michalski (2016) previously used an *ab initio* approach to determine an

280  $\alpha_2$  value of 0.9933 at room temperature, 0.9943 at 237 K and 0.9929 at 310 K. The total variation  
281 of  $\alpha_2$  values from 273 K to 310 K is only 1.4 ‰, significantly smaller than our experimental  
282 uncertainty ( $\pm 5$  ‰). The  $\alpha_1$  value was calculated using a ZPE shift model (Miller & Yung, 2000)  
283 to calculate the isotopic fractionation of NO<sub>2</sub> by photolysis. Briefly, this model assumes both  
284 isotopologues have the same quantum yield function and the PHIFE was only caused by the  
285 differences in the <sup>15</sup>NO<sub>2</sub> and <sup>14</sup>NO<sub>2</sub> absorption cross-section as a function of wavelength, thus  $\alpha_1$   
286 values do not vary by temperature. The <sup>15</sup>NO<sub>2</sub> absorption cross-section was calculated by shifting  
287 the <sup>14</sup>NO<sub>2</sub> absorption cross-section by the <sup>15</sup>NO<sub>2</sub> zero-point energy (Michalski et al., 2004). When  
288 the ZPE shift model was used with the irradiation spectrum of the chamber lights, the resulting  $\alpha_1$   
289 value was 1.0023. Therefore, the theoretically predicted  $\alpha_2 - \alpha_1$  value should be -0.0090, i.e., (-  
290 9.0 $\pm$ 0.7) ‰ when temperature ranges from 273 K to 310 K. This result shows excellent agreement  
291 with our experimentally determined room temperature  $\alpha_2 - \alpha_1$  value of (-10 $\pm$ 5) ‰.

292 This model was then used to evaluate the variations of  $\alpha_1$  value to different lighting  
293 conditions. The TUV model (TUV5.3.2, Madronich & Flocke, 1999) was used to calculate the  
294 solar wavelength spectrum at three different conditions: early morning/late afternoon (solar zenith  
295 angle=85 degree), mid-morning/afternoon (solar zenith angle=45 degree), noon (solar zenith  
296 angle=0 degree). These spectrums were used in the ZPE shift model to calculate the  $\alpha_1$  values,  
297 which are 1.0025, 1.0028, and 1.0029 at solar zenith angles of 85, 45 and 0 degree, respectively.  
298 These values, along with the predicted  $\alpha_1$  value in the chamber, showed a total span of 0.6‰  
299 (1.0026 $\pm$ 0.0003), which is again significantly smaller than our measured uncertainty. Therefore,  
300 we suggest that our experimentally determined LCIE factor ((-10 $\pm$ 5) ‰) can be used in most  
301 tropospheric solar irradiation spectrums.

302 The equations can also be applied in tropospheric environments to calculate the combined  
303 isotopic fractionations of EIE and LCIE for NO and NO<sub>2</sub>. First, the NO<sub>2</sub> sink reactions (mainly  
304 NO<sub>2</sub>+OH in the daytime) are at least 2-3 orders of magnitude slower than the Leighton cycle and  
305 the NO-NO<sub>2</sub> isotope exchange reactions (Walters et al., 2016), therefore their effects on the δ(NO<sub>2</sub>)  
306 should be minor. Second, although the conversion of NO into NO<sub>2</sub> in the ambient environment is  
307 also controlled by NO + RO<sub>2</sub> and HO<sub>2</sub> in addition to NO+O<sub>3</sub> (e.g., King et al., 2001), Eq. (7) still  
308 showed good agreement with field observations in previous studies. Freyer et al. (1993)  
309 determined the annual average daytime δ(NO<sub>2</sub>)-δ(NO) at Julich, Germany along with average  
310 daytime NO concentration (9 nmol mol<sup>-1</sup>, similar to our experimental conditions) to be  
311 (+18.03±0.98) ‰. Using Eq. (7), assuming the daytime average *j*(NO<sub>2</sub>) value throughout the year  
312 was (5.0±1.0)×10<sup>-3</sup>, and a calculated A value from measured NO<sub>x</sub> concentration ranged from 0.22-  
313 0.33, the average NO-NO<sub>2</sub> fractionation factor was calculated to be (+19.8±1.4) ‰ (Fig. 1C), in  
314 excellent agreement with the measurements in the present study. This agreement suggests the  
315 NO+RO<sub>2</sub>/HO<sub>2</sub> reactions might have similar fractionation factors as NO+O<sub>3</sub>. Therefore, we suggest  
316 Eq. (7) and (8) can be used to estimate the isotopic fractionations between NO and NO<sub>2</sub> in the  
317 troposphere.

318

### 319 **3.3 Calculating nitrogen isotopic fractionations of NO-NO<sub>2</sub>**

320 First, Eq. (7) was used to calculate the Δ(NO<sub>2</sub>-NO) = δ(NO<sub>2</sub>)-δ(NO) at a wide range of  
321 NO<sub>x</sub> concentrations, *f*(NO<sub>2</sub>) and *j*(NO<sub>2</sub>) values (Fig. 2A-D), assuming (1+δ(NO<sub>2</sub>)) ≈ 1. *j*(NO<sub>2</sub>)  
322 values of 0 s<sup>-1</sup> (Fig. 2A), 1.4×10<sup>-3</sup> s<sup>-1</sup> (Fig. 2B), 5×10<sup>-3</sup> s<sup>-1</sup> (Fig. 2C) and 1×10<sup>-2</sup> s<sup>-1</sup> (Fig. 2D) were  
323 selected to represent nighttime, dawn (as well as the laboratory conditions of our experiments),  
324 daytime average and noon, respectively. Each panel represented a fixed *j*(NO<sub>2</sub>) value, and the

325  $\Delta(\text{NO}_2\text{-NO})$  values were calculated as a function of the A value, which was derived from  $\text{NO}_x$   
326 concentration and  $f(\text{NO}_2)$ . The A values have a large span, from 0 to 500, depending on the  $j(\text{NO}_2)$   
327 value and the NO concentration. When  $A=0$  ( $j(\text{NO}_2)=0$ ) and  $f(\text{NO}_2)<1$  (meaning NO- $\text{NO}_2$  coexist  
328 and  $[\text{O}_3]=0$ ), Eq. (7) and (8) become Eq. (2) and (3), showing the EIE was the sole factor, the  
329  $\Delta(\text{NO}_2\text{-NO})$  values were solely controlled by EIE which has a constant value of +28.9 ‰ at 298K  
330 (Fig. 2A). When  $j(\text{NO}_2)>0$ , the calculated  $\Delta(\text{NO}_2\text{-NO})$  values showed a wide range from -10.0 ‰  
331 (controlled by LCIE factor:  $\alpha_2-\alpha_1=-10$  ‰) to +28.9 ‰ (controlled by EIE factor:  $\alpha(\text{NO}_2\text{-NO})-1 =$   
332 +28.9 ‰). Fig. 2B-D display the transition from a LCIE-dominated regime to an EIE-dominated  
333 regime. The LCIE-dominated regime is characterized by low  $[\text{NO}_x]$  ( $<50$  pmol mol<sup>-1</sup>), representing  
334 remote ocean areas and polar regions (Beine et al., 2002; Custard et al., 2015). At this range the A  
335 value can be greater than 200, thus Eq. (7) can be simplified as:  $\Delta(\text{NO}_2\text{-NO}) = \alpha_2-\alpha_1$ , suggesting  
336 the LCIE almost exclusively controls the NO- $\text{NO}_2$  isotopic fractionation. The  $\Delta(\text{NO}_2\text{-NO})$  values  
337 of these regions are predicted to be  $<0$  ‰ during most time of the day and  $< -5$  ‰ at noon. On the  
338 other hand, the EIE-dominated regime was characterized by high  $[\text{NO}_x]$  ( $>20$  nmol mol<sup>-1</sup>) and low  
339  $f(\text{NO}_2)$  ( $< 0.6$ ), representative of regions with intensive NO emissions, e.g., near roadside or stack  
340 plumes (Clapp & Jenkin, 2001; Kimbrough et al., 2017). In this case, the  $\tau_{\text{exchange}}$  are relatively  
341 short (10-50 s) compared to the  $\tau_{\text{photo}}$  (approximately 100 s at noon and 1000 s at dawn), therefore  
342 the A values are small (0.01-0.5). The EIE factor in this regime thus is much more important than  
343 the LCIE factor, resulting in high  $\Delta(\text{NO}_2\text{-NO})$  values ( $>20$  ‰). Between the two regimes, both  
344 EIE and LCIE are competitive and therefore it is necessary to use Eq. (7) to quantify the  $\Delta(\text{NO}_2\text{-}$   
345 NO) values.

346 Fig. 2 also implies that changes in the  $j(\text{NO}_2)$  value can cause the diurnal variations in  
347  $\Delta(\text{NO}_2\text{-NO})$  values. Changing  $j(\text{NO}_2)$  would affect the value of A and consequently the NO- $\text{NO}_2$

348 isotopic fractionations in two ways: 1) changes in  $j(\text{NO}_2)$  value would change the photolysis  
349 intensity, therefore the  $\tau_{\text{photo}}$  value; 2) in addition, changes in  $j(\text{NO}_2)$  value would also alter the  
350 steady state NO concentration, therefore changing the  $\tau_{\text{exchange}}$  (Fig. 2C). The combined effect of  
351 these two factors on the A value varies along with the atmospheric conditions, and thus needs to  
352 be carefully calculated using  $\text{NO}_x$  concentration data and atmospheric chemistry models.

353 We then calculated the differences of  $\delta^{15}\text{N}$  values between  $\text{NO}_2$  and total  $\text{NO}_x$ , e.g.  $\Delta(\text{NO}_2-$   
354  $\text{NO}_x) = \delta(\text{NO}_2) - \delta(\text{NO}_x)$  in Fig. 2E-H. Since  $\Delta(\text{NO}_2-\text{NO}_x)$  are connected through the observed  $\delta^{15}\text{N}$   
355 of  $\text{NO}_2$  (or nitrate) to the  $\delta^{15}\text{N}$  of  $\text{NO}_x$  sources, this term might be useful in field studies (e.g.,  
356 Chang et al., 2018; Zong et al., 2017). The calculated  $\Delta(\text{NO}_2-\text{NO}_x)$  values (Fig. 2E-H) also showed  
357 a LCIE-dominated regime at low  $[\text{NO}_x]$  and an EIE-dominated regime at high  $[\text{NO}_x]$ . The  $\Delta(\text{NO}_2-$   
358  $\text{NO}_x)$  values were dampened by the  $1-f(\text{NO}_2)$  factor comparing to  $\Delta(\text{NO}_2-\text{NO})$ , as shown in Eq.  
359 (3) and (8):  $\Delta(\text{NO}_2-\text{NO}_x) = \Delta(\text{NO}_2-\text{NO}) (1-f(\text{NO}_2))$ . At high  $f(\text{NO}_2)$  values ( $>0.8$ ), the differences  
360 between  $\delta(\text{NO}_2)$  and  $\delta(\text{NO}_x)$  were less than 5 ‰, thus the measured  $\delta(\text{NO}_2)$  values were similar to  
361  $\delta(\text{NO}_x)$ , although the isotopic fractionation between NO and  $\text{NO}_2$  could be noteworthy. Some  
362 ambient environments with significant NO emissions or high  $\text{NO}_2$  photolysis rates usually have  
363  $f(\text{NO}_2)$  values between 0.4-0.8 (Mazzeo et al., 2005; Vicars et al., 2013). In this scenario, the  
364  $\Delta(\text{NO}_2-\text{NO}_x)$  values in Fig. 2F-H showed wide ranges of -4.8 ‰ to +15.6 ‰, -6.0 ‰ to +15.0 ‰,  
365 and -6.3 ‰ to +14.2 ‰ at  $j(\text{NO}_2)=1.4\times 10^{-3} \text{ s}^{-1}$ ,  $5\times 10^{-3} \text{ s}^{-1}$ ,  $1\times 10^{-2} \text{ s}^{-1}$ , respectively. These significant  
366 differences again highlighted the importance of both LCIE and EIE (Eq. (7) and (8)) in calculating  
367 the  $\Delta(\text{NO}_2-\text{NO}_x)$ . In the following discussion, we assume 1) the  $\alpha_1$  value remain constant (see  
368 discussion above), 2) the  $\text{NO}+\text{RO}_2/\text{HO}_2$  reactions have the same fractionation factors ( $\alpha_2$ ) as  
369  $\text{NO}+\text{O}_3$ , and 3) both EIE and LCIE do not display significant temperature dependence, then use



370 Equations (7) and (8) and this laboratory determined LCIE factor (-10 ‰) to calculate the nitrogen  
371 isotopic fractionation between NO and NO<sub>2</sub> at various tropospheric atmospheric conditions.

372

#### 373 **4. Implications**

374 The daily variations of  $\Delta(\text{NO}_2\text{-NO}_x)$  values at two roadside NO<sub>x</sub> monitoring sites were  
375 predicted to demonstrate the effects of NO<sub>x</sub> concentrations to the NO-NO<sub>2</sub> isotopic fractionations.  
376 Hourly NO and NO<sub>2</sub> concentrations were acquired from a roadside site at Anaheim, CA  
377 (<https://www.arb.ca.gov>) and an urban site at Evansville, IN (<http://idem.tx.sutron.com>) on July  
378 25, 2018. The hourly  $j(\text{NO}_2)$  values output from the TUV model (Madronich & Flocke, 1999) at  
379 these locations was used to calculate the daily variations of  $\Delta(\text{NO}_2\text{-NO}_x)$  values (Fig. 3A, B) by  
380 applying Eq. (8) and assuming  $(1+\delta(\text{NO}_2)) \approx 1$ . Hourly NO<sub>x</sub> concentrations were 12-51 nmol mol<sup>-1</sup>  
381 <sup>1</sup> at Anaheim and 9-38 nmol mol<sup>-1</sup> at Evansville and the  $f(\text{NO}_2)$  values at both sites did not show  
382 significant daily variations ( $0.45 \pm 0.07$  at Anaheim and  $0.65 \pm 0.08$  at Evansville), likely because  
383 the NO<sub>x</sub> concentrations were controlled by the high NO emissions from the road (Gao, 2007). The  
384 calculated  $\Delta(\text{NO}_2\text{-NO}_x)$  values using Eq. (8) showed significant diurnal variations. During the  
385 nighttime, the isotopic fractionations were solely controlled by the EIE, the predicted  $\Delta(\text{NO}_2\text{-NO}_x)$   
386 values were  $(+14.5 \pm 2.0)$  ‰ and  $(+8.7 \pm 2.1)$  ‰ at Anaheim and Evansville, respectively. During  
387 the daytime, the existence of LCIE lowered the predicted  $\Delta(\text{NO}_2\text{-NO}_x)$  values to  $(+9.8 \pm 1.7)$  ‰ at  
388 Anaheim and  $(+3.1 \pm 1.5)$  ‰ at Evansville while the  $f(\text{NO}_2)$  values at both sites remained similar.  
389 The lowest  $\Delta(\text{NO}_2\text{-NO}_x)$  values for both sites  $(+7.0)$  ‰ and  $(+1.7)$  ‰ occurred around noon when  
390 the NO<sub>x</sub> photolysis was the most intense. In contrast, if one neglects the LCIE factor in the daytime,  
391 the  $\Delta(\text{NO}_2\text{-NO}_x)$  values would be  $(+12.9 \pm 1.5)$  ‰ and  $(+10.0 \pm 1.6)$  ‰ respectively, an  
392 overestimation of 3.1 ‰ and 6.9 ‰. These discrepancies suggested that the LCIE played an

393 important role in the NO-NO<sub>2</sub> isotopic fractionations and neglecting it could bias the NO<sub>x</sub> source  
394 apportionment using  $\delta^{15}\text{N}$  of NO<sub>2</sub> or nitrate.

395 The role of LCIE was more important in less polluted sites. The  $\Delta(\text{NO}_2\text{-NO}_x)$  values  
396 calculated for a suburban site near San Diego, CA, USA, again using the hourly NO<sub>x</sub>  
397 concentrations (<https://www.arb.ca.gov>, Fig. 3C) and  $j(\text{NO}_2)$  values calculated from the TUV  
398 model. NO<sub>x</sub> concentrations at this site varied from 1 to 9 nmol mol<sup>-1</sup> and assuming  $(1+\delta(\text{NO}_2)) \approx 1$ .  
399 During the nighttime, NO<sub>x</sub> was in the form of NO<sub>2</sub> ( $f(\text{NO}_2) = 1$ ) because O<sub>3</sub> concentrations were  
400 higher than NO<sub>x</sub>, thus the  $\delta(\text{NO}_2)$  values should be identical to  $\delta(\text{NO}_x)$  ( $\Delta(\text{NO}_2\text{-NO}_x) = 0$ ). In the  
401 daytime a certain amount of NO was produced by direct NO emission and NO<sub>2</sub> photolysis but the  
402  $f(\text{NO}_2)$  was still high ( $0.73 \pm 0.08$ ). Our calculation suggested the daytime  $\Delta(\text{NO}_2\text{-NO}_x)$  values  
403 should be only  $(+1.3 \pm 3.2)$  ‰ with a lowest value of -1.3 ‰. These  $\Delta(\text{NO}_2\text{-NO}_x)$  values were  
404 similar to the observed and modeled summer daytime  $\delta(\text{NO}_2)$  values in West Lafayette, IN  
405 (Walters et al., 2018), which suggest the average daytime  $\Delta(\text{NO}_2\text{-NO}_x)$  values at NO<sub>x</sub> =  $(3.9 \pm 1.2)$   
406 nmol mol<sup>-1</sup> should range from +0.1 ‰ to +2.4 ‰. In this regime, we suggest the  $\Delta(\text{NO}_2\text{-NO}_x)$   
407 values were generally small due to the significant contribution of LCIE and high  $f(\text{NO}_2)$ .

408 The LCIE should be the dominant factor controlling the NO-NO<sub>2</sub> isotopic fractionation at  
409 remote regions, resulting in a completely different diurnal pattern of  $\Delta(\text{NO}_2\text{-NO}_x)$  compared with  
410 the urban-suburban area. Direct hourly measurements of NO<sub>x</sub> at remote sites are rare, thus we used  
411 total NO<sub>x</sub> concentration of 50 pmol mol<sup>-1</sup>, daily O<sub>3</sub> concentration of 20 nmol mol<sup>-1</sup> at Summit,  
412 Greenland (Dibb et al., 2002; Hastings et al., 2004; Honrath et al., 1999; Yang et al., 2002), and  
413 assumed  $(1+\delta(\text{NO}_2)) \approx 1$  and the conversion of NO to NO<sub>2</sub> was completely controlled by O<sub>3</sub> to  
414 calculate the NO/NO<sub>2</sub> ratios. Here the isotopes of NO<sub>x</sub> were almost exclusively controlled by the  
415 LCIE due to the high A values ( $>110$ ). The  $\Delta(\text{NO}_2\text{-NO}_x)$  values displayed a clear diurnal pattern

416 (Fig. 3D) with highest value of -0.3 ‰ in the “nighttime” (solar zenith angle >85 degree) and  
417 lowest value of -5.0 ‰ in the mid-day. This suggest that the isotopic fractionations between NO  
418 and NO<sub>2</sub> were almost completely controlled by LCIE at remote regions, when NO<sub>x</sub> concentrations  
419 were <0.1 nmol mol<sup>-1</sup>. However, since the isotopic fractionation factors of nitrate-formation  
420 reactions (NO<sub>2</sub>+OH, NO<sub>3</sub>+HC, N<sub>2</sub>O<sub>5</sub>+H<sub>2</sub>O) are still unknown, more studies are needed to fully  
421 explain the daily and seasonal variations of δ(NO<sub>3</sub><sup>-</sup>) at remote regions.

422         Nevertheless, our results have a few limitations. First, currently there are very few field  
423 observations that can be used to evaluate our model, therefore, future field observations that  
424 measure the δ<sup>15</sup>N values of ambient NO and NO<sub>2</sub> should be carried out to test our model. Second,  
425 more work, including theoretical and experimental studies, is needed to investigate the isotope  
426 fractionation factors occurring during the conversion from NO<sub>x</sub> to NO<sub>y</sub> and nitrate: in the NO<sub>y</sub>  
427 cycle, EIE (isotopic exchange between NO<sub>2</sub>, NO<sub>3</sub> and N<sub>2</sub>O<sub>5</sub>), KIE (formation of NO<sub>3</sub>, N<sub>2</sub>O<sub>5</sub> and  
428 nitrate) and PHIFE (photolysis of NO<sub>3</sub>, N<sub>2</sub>O<sub>5</sub>, HONO and sometimes nitrate) may also exist and  
429 be relevant for the δ<sup>15</sup>N of HNO<sub>3</sub> and HONO. In particular, the N isotope fractionation occurring  
430 during the NO<sub>2</sub> + OH → HNO<sub>3</sub> reaction needs investigation. Such studies could help us modeling  
431 the isotopic fractionation between NO<sub>x</sub> emission and nitrate, and eventually enable us to analyze  
432 the δ<sup>15</sup>N value of NO<sub>x</sub> emission by measuring the δ<sup>15</sup>N values of nitrate aerosols and nitrate in wet  
433 depositions. Third, our discussion only focuses on the reactive nitrogen chemistry in the  
434 troposphere, however, the nitrogen chemistry in the stratosphere is drastically different from the  
435 tropospheric chemistry, thus future studies are also needed to investigate the isotopic fractionations  
436 in the stratospheric nitrogen chemistry. Last, the temperature dependence of both EIE and LCIE  
437 needs to be carefully investigated, because of the wide range of temperature in both troposphere  
438 and stratosphere. Changes in temperature could alter the isotopic fractionation factors of both EIE

439 and LCIE, as well as contribute to the seasonality of isotopic fractionations between  $\text{NO}_x$  and  $\text{NO}_y$   
440 molecules.

441

## 442 **5. Conclusions**

443 The effect of  $\text{NO}_x$  photochemistry on the nitrogen isotopic fractionations between NO and  
444  $\text{NO}_2$  was investigated. We first measured the isotopic fractionations between NO and  $\text{NO}_2$  and  
445 provided mathematical solutions to assess the impact of  $\text{NO}_x$  level and  $\text{NO}_2$  photolysis rate ( $j(\text{NO}_2)$ )  
446 to the relative importance of EIE and LCIE. The EIE and LCIE isotope fractionation factors, at  
447 room temperature, were determined to be  $1.0289 \pm 0.0019$  and  $0.990 \pm 0.005$ , respectively. These  
448 calculations and measurements can be used to determine the steady state  $\Delta(\text{NO}_2\text{-NO})$  and  $\Delta(\text{NO}_2\text{-}$   
449  $\text{NO}_x)$  values at room temperature. Subsequently we applied our equations to polluted, clean and  
450 remote sites to model the daily variations of  $\Delta(\text{NO}_2\text{-NO}_x)$  values. We found that the  $\Delta(\text{NO}_2\text{-NO}_x)$   
451 values could vary from over +20 ‰ to less than -5 ‰ depending on the environment: in general,  
452 the role of LCIE becoming more important at low  $\text{NO}_x$  concentrations, which tend to decrease the  
453  $\Delta(\text{NO}_2\text{-NO}_x)$  values. Our work provided a mathematical approach to quantify the nitrogen isotopic  
454 fractionations between NO and  $\text{NO}_2$  that can be applied to many tropospheric environments, which  
455 could help interpret the measured  $\delta^{15}\text{N}$  values of  $\text{NO}_2$  and nitrate in field observation studies.

456

## 457 **Acknowledgement**

458 We thank NCAR's Advanced Study Program granted to Jianghanyang Li. The National  
459 Center for Atmospheric Research is operated by the University Corporation for Atmospheric  
460 Research, under the sponsorship of the National Science Foundation. We also thank funding

461 support from Purdue Climate Change Research Center and A. H. Ismail Interdisciplinary Program  
462 Doctoral Research Travel Award granted by Purdue University.

### 463 **Data Availability**

464 Data acquired from this study was deposited at Open Sciences Framework (Li, 2019,  
465 DOI 10.17605/OSF.IO/JW8HU).

### 466 **Author contribution**

467 J. Li and G. Michalski designed the experiments, X. Zhang and J. Li conducted the  
468 experiments. X. Zhang, G. Michalski, J. Orlando and G. Tyndall helped J. Li in interpreting the  
469 results. The manuscript was written by J. Li and all the authors have contributed during the revision  
470 of this manuscript.

### 471 **Competing interest**

472 The authors declare no competing interest.

473

### 474 **References:**

475  
476 Atkinson, R., Baulch, D. L., Cox, R. A., Crowley, J. N., Hampson, R. F., Hynes, R. G., Jenkin, M.  
477 E., Rossi, M. J., and Troe, J. (2004). Evaluated kinetic and photochemical data for atmospheric  
478 chemistry: Volume I-gas phase reactions of O<sub>x</sub>, HO<sub>x</sub>, NO<sub>x</sub> and SO<sub>x</sub>. *Atmospheric chemistry and*  
479 *physics*, 4(6), 1461-1738. <https://doi.org/10.5194/acp-4-1461-2004>, 2004.

480  
481 Barney, W. S., & Finlayson-Pitts, B. J. (2000). Enhancement of N<sub>2</sub>O<sub>4</sub> on porous glass at room  
482 temperature: A key intermediate in the heterogeneous hydrolysis of NO<sub>2</sub>? *The Journal of Physical*  
483 *Chemistry A*, 104(2), 171–175. <https://doi.org/10.1021/jp993169b>

484  
485 Begun, G. M., & Fletcher, W. H. (1960). Partition function ratios for molecules containing  
486 nitrogen isotopes. *The Journal of Chemical Physics*, 33(4), 1083–1085.  
487 <https://doi.org/10.1063/1.1731338>

488  
489 Begun, G. M., & Melton, C. E. (1956). Nitrogen isotopic fractionation between NO and NO<sub>2</sub> and  
490 mass discrimination in mass analysis of NO<sub>2</sub>. *The Journal of Chemical Physics*, 25(6), 1292–1293.  
491 <https://doi.org/10.1063/1.1743215>

492

493 Beine, H. J., Honrath, R. E., Dominé, F., Simpson, W. R., & Fuentes, J. D. (2002). NO<sub>x</sub> during  
494 background and ozone depletion periods at Alert: Fluxes above the snow surface. *Journal of*  
495 *Geophysical Research: Atmospheres*, 107(D21), ACH-7. <https://doi.org/10.1029/2002JD002082>  
496

497 Bigeleisen, J., & Mayer, M. G. (1947). Calculation of equilibrium constants for isotopic exchange  
498 reactions. *The Journal of Chemical Physics*, 15(5), 261-267. <https://doi.org/10.1063/1.1746492>  
499

500 Bigeleisen, J., & Wolfsberg, M. (1957). Theoretical and experimental aspects of isotope effects in  
501 chemical kinetics. *Advances in Chemical Physics*, 15-76.  
502 <https://doi.org/10.1002/9780470143476.ch2>  
503

504 Casciotti, K. L., & McIlvin, M. R. (2007). Isotopic analyses of nitrate and nitrite from reference  
505 mixtures and application to Eastern Tropical North Pacific waters. *Marine Chemistry*, 107(2), 184-  
506 201. <https://doi.org/10.1016/j.marchem.2007.06.021>  
507

508 Chang, Y., Zhang, Y., Tian, C., Zhang, S., Ma, X., Cao, F., et al. (2018). Nitrogen isotope  
509 fractionation during gas-to-particle conversion of NO<sub>x</sub> to NO<sub>3</sub><sup>-</sup> in the atmosphere—implications for  
510 isotope-based NO<sub>x</sub> source apportionment. *Atmospheric Chemistry and Physics*, 18(16), 11647-  
511 11661. <https://doi.org/10.5194/acp-18-11647-2018>, 2018.  
512

513 Clapp, L. J., & Jenkin, M. E. (2001). Analysis of the relationship between ambient levels of O<sub>3</sub>,  
514 NO<sub>2</sub> and NO as a function of NO<sub>x</sub> in the UK. *Atmospheric Environment*, 35(36), 6391-6405.  
515 [https://doi.org/10.1016/S1352-2310\(01\)00378-8](https://doi.org/10.1016/S1352-2310(01)00378-8)  
516

517 Custard, K. D., Thompson, C. R., Pratt, K. A., Shepson, P. B., Liao, J., Huey, L. G., Orlando, J. J.,  
518 Weinheimer, A. J., Apel, E., Hall, S. R., Flocke, F., Mauldin, L., Hornbrook, R. S., Pöhler, D.,  
519 General, S., Zielcke, J., Simpson, W. R., Platt, U., Fried, A., Weibring, P., Sive, B. C., Ullmann,  
520 K., Cantrell, C., Knapp, D. J., and Montzka, D. D.: The NO<sub>x</sub> dependence of bromine chemistry in  
521 the Arctic atmospheric boundary layer, *Atmos. Chem. Phys.*, 15, 10799-10809,  
522 <https://doi.org/10.5194/acp-15-10799-2015>, 2015.  
523

524 Dibb, J. E., Arsenault, M., Peterson, M. C., & Honrath, R. E. (2002). Fast nitrogen oxide  
525 photochemistry in Summit, Greenland snow. *Atmospheric Environment*, 36(15-16), 2501-2511.  
526 [https://doi.org/10.1016/S1352-2310\(02\)00130-9](https://doi.org/10.1016/S1352-2310(02)00130-9)  
527

528 Do Remus, R. H., Mehrotra, Y., Lanford, W. A., & Burman, C. (1983). Reaction of water with  
529 glass: influence of a transformed surface layer. *Journal of Materials Science*, 18(2), 612-622.  
530 <https://doi.org/10.1007/BF00560651>  
531

532 Elliott, E. M., Kendall, C., Boyer, E. W., Burns, D. A., Lear, G. G., Golden, H. E., Harlin, K.,  
533 Bytnerowicz, A., Butler, T. J., and Glatz, R. (2009). Dual nitrate isotopes in dry deposition: Utility  
534 for partitioning NO<sub>x</sub> source contributions to landscape nitrogen deposition. *Journal of Geophysical*  
535 *Research: Biogeosciences*, 114(G4), G04020. <https://doi.org/10.1029/2008JG000889>  
536

537 Felix, J. D., & Elliott, E. M. (2014). Isotopic composition of passively collected nitrogen dioxide  
538 emissions: Vehicle, soil and livestock source signatures. *Atmospheric Environment*, 92, 359–366.  
539 <https://doi.org/10.1016/j.atmosenv.2014.04.005>  
540

541 Felix, J. D., Elliott, E. M., & Shaw, S. L. (2012). Nitrogen isotopic composition of coal-fired power  
542 plant NO<sub>x</sub>: influence of emission controls and implications for global emission inventories.  
543 *Environmental Science & Technology*, 46(6), 3528–3535. <https://doi.org/10.1021/es203355v>  
544

545 Frey, M. M., Savarino, J., Morin, S., Erbland, J., & Martins, J. M. F. (2009). Photolysis imprint in  
546 the nitrate stable isotope signal in snow and atmosphere of East Antarctica and implications for  
547 reactive nitrogen cycling. *Atmos. Chem. Phys*, 9, 8681–8696. [https://doi.org/10.5194/acp-9-8681-](https://doi.org/10.5194/acp-9-8681-2009)  
548 2009, 2009.  
549

550 Freyer, H. D. (1991). Seasonal variation of <sup>15</sup>N/<sup>14</sup>N ratios in atmospheric nitrate species. *Tellus B*,  
551 43(1), 30–44. <https://doi.org/10.1034/j.1600-0889.1991.00003.x>  
552

553 Freyer, H. D., Kley, D., Volz-Thomas, A., & Kobel, K. (1993). On the interaction of isotopic  
554 exchange processes with photochemical reactions in atmospheric oxides of nitrogen. *Journal of*  
555 *Geophysical Research: Atmospheres*, 98(D8), 14791–14796. <https://doi.org/10.1029/93JD00874>  
556

557 Gao, H. O. (2007). Day of week effects on diurnal ozone/NO<sub>x</sub> cycles and transportation emissions  
558 in Southern California. *Transportation Research Part D: Transport and Environment*, 12(4), 292–  
559 305. <https://doi.org/10.1016/j.trd.2007.03.004>  
560

561 Gobel, A. R., Altieri, K. E., Peters, A. J., Hastings, M. G., & Sigman, D. M. (2013). Insights into  
562 anthropogenic nitrogen deposition to the North Atlantic investigated using the isotopic  
563 composition of aerosol and rainwater nitrate. *Geophysical Research Letters*, 40(22), 5977–5982.  
564 <https://doi.org/10.1002/2013GL058167>  
565

566 Hastings, M G, Jarvis, J. C., & Steig, E. J. (2009). Anthropogenic impacts on nitrogen isotopes of  
567 ice-core nitrate. *Science*, 324(5932), 1288. DOI: 10.1126/science.1170510  
568

569 Hastings, M G, Steig, E. J., & Sigman, D. M. (2004). Seasonal variations in N and O isotopes of  
570 nitrate in snow at Summit, Greenland: Implications for the study of nitrate in snow and ice cores.  
571 *Journal of Geophysical Research: Atmospheres*, 109(D20).  
572 <https://doi.org/10.1029/2004JD004991>  
573

574 Honrath, R. E., Peterson, M. C., Guo, S., Dibb, J. E., Shepson, P. B., & Campbell, B. (1999).  
575 Evidence of NO<sub>x</sub> production within or upon ice particles in the Greenland snowpack. *Geophysical*  
576 *Research Letters*, 26(6), 695–698. <https://doi.org/10.1029/1999GL900077>  
577

578 Jarvis, J. C., Steig, E. J., Hastings, M. G., & Kunasek, S. A. (2008). Influence of local  
579 photochemistry on isotopes of nitrate in Greenland snow. *Geophysical Research Letters*, 35(21).  
580 <https://doi.org/10.1029/2008GL035551>  
581

582 Kendall, C., Elliott, E. M., & Wankel, S. D. (2007). Tracing anthropogenic inputs of nitrogen to  
583 ecosystems. *Stable Isotopes in Ecology and Environmental Science*, 2, 375–449.  
584 <https://doi.org/10.1002/9780470691854.ch12>  
585

586 Kimbrough, S., Owen, R. C., Snyder, M., & Richmond-Bryant, J. (2017). NO to NO<sub>2</sub> conversion  
587 rate analysis and implications for dispersion model chemistry methods using Las Vegas, Nevada  
588 near-road field measurements. *Atmospheric Environment*, 165, 23–34.  
589 <https://doi.org/10.1016/j.atmosenv.2017.06.027>  
590

591 King, M. D., Canosa-Mas, C. E. and Wayne R. P. (2001). Gas-phase reactions between RO<sub>2</sub> and  
592 NO, HO<sub>2</sub> or CH<sub>3</sub>O<sub>2</sub>: correlations between rate constants and the SOMO energy of the peroxy (RO<sub>2</sub>)  
593 radical. *Atmospheric Environment* 35.12 (2001): 2081-2088. [https://doi.org/10.1016/S1352-  
594 2310\(00\)00501-X](https://doi.org/10.1016/S1352-2310(00)00501-X)  
595

596 Knote, C., Tuccella, P., Curci, G., Emmons, L., Orlando, J. J. Madronich, S., Baró, R., Jiménez-  
597 Guerrero, P., Luecken, D., Hogrefe, C., Forkel, R., Werhahn, J., Hirtl, M., Pérez, J. L., San José,  
598 R., Giordano, L., Brunner, D., Yahya, K., Zhang, Y., Influence of the choice of gas-phase  
599 mechanism on predictions of key gaseous pollutants during the AQMEII phase-2 intercomparison.  
600 *Atmospheric Environment* 115 (2015): 553-568. <https://doi.org/10.1016/j.atmosenv.2014.11.066>.  
601

602 Li, J. (2019). Quantifying the nitrogen equilibrium and photochemistry-induced kinetic isotopic  
603 effects between NO and NO<sub>2</sub>. Retrieved from [osf.io/jw8hu](https://osf.io/jw8hu)  
604

605 Madronich, S., & Flocke, S. (1999). The role of solar radiation in atmospheric chemistry. In  
606 *Environmental photochemistry* (pp. 1–26). *The Handbook of Environmental Chemistry (Reactions  
607 and Processes)*, vol 2 / 2L. Springer, Berlin, Heidelberg. [https://doi.org/10.1007/978-3-540-69044-  
608 3\\_1](https://doi.org/10.1007/978-3-540-69044-3_1)  
609

610 Mazzeo, N. A., Venegas, L. E., & Choren, H. (2005). Analysis of NO, NO<sub>2</sub>, O<sub>3</sub> and NO<sub>x</sub>  
611 concentrations measured at a green area of Buenos Aires City during wintertime. *Atmospheric  
612 Environment*, 39(17), 3055–3068. <https://doi.org/10.1016/j.atmosenv.2005.01.029>  
613

614 McIlvin, M. R., & Altabet, M. A. (2005). Chemical conversion of nitrate and nitrite to nitrous  
615 oxide for nitrogen and oxygen isotopic analysis in freshwater and seawater. *Analytical Chemistry*,  
616 77(17), 5589–5595. <https://doi.org/10.1021/ac050528s>  
617

618 Michalski, G., Jost, R., Sugny, D., Joyeux, M., & Thiemens, M. (2004). Dissociation energies of  
619 six NO<sub>2</sub> isotopologues by laser induced fluorescence spectroscopy and zero-point energy of some  
620 triatomic molecules. *The Journal of Chemical Physics*, 121(15), 7153–7161.  
621 <https://doi.org/10.1063/1.1792233>  
622

623 Michalski, G., Bockheim, J. G., Kendall, C., & Thiemens, M. (2005). Isotopic composition of  
624 Antarctic Dry Valley nitrate: Implications for NO<sub>y</sub> sources and cycling in Antarctica. *Geophysical  
625 Research Letters*, 32(13). <https://doi.org/10.1029/2004GL022121>  
626



627 Miller, C. E., & Yung, Y. L. (2000). Photo-induced isotopic fractionation. *Journal of Geophysical*  
628 *Research: Atmospheres*, 105(D23), 29039–29051. <https://doi.org/10.1029/2000JD900388>  
629

630 Monse, E. U., Spindel, W., & Stern, M. J. (1969). Analysis of isotope-effect calculations illustrated  
631 with exchange equilibria among oxynitrogen compounds. Rutgers-The State Univ., Newark, NJ.  
632 DOI: 10.1021/ba-1969-0089.ch009  
633

634 Morin, S., Savarino, J., Frey, M. M., Domine, F., Jacobi, H.-W., Kaleschke, L., & Martins, J. M.  
635 F. (2009). Comprehensive isotopic composition of atmospheric nitrate in the Atlantic Ocean  
636 boundary layer from 65°S to 79°N. *J. Geophys. Res.*, 114. <https://doi.org/10.1029/2008JD010696>  
637

638 Park, Y.-M., Park, K.-S., Kim, H., Yu, S.-M., Noh, S., Kim, M.-S., Kim, J.-Y., Ahn, J.-Y., Lee,  
639 M.-D., Seok, K.-S., Kin, Y.-H., (2018). Characterizing isotopic compositions of TC-C, NO<sub>3</sub><sup>-</sup>-N,  
640 and NH<sub>4</sub><sup>+</sup>-N in PM<sub>2.5</sub> in South Korea: Impact of China's winter heating.  
641 <https://doi.org/10.1016/j.envpol.2017.10.072>  
642

643 Saliba, N. A., Yang, H., & Finlayson-Pitts, B. J. (2001). Reaction of gaseous nitric oxide with  
644 nitric acid on silica surfaces in the presence of water at room temperature. *The Journal of Physical*  
645 *Chemistry A*, 105(45), 10339–10346. <https://doi.org/10.1021/jp012330r>  
646

647 Savarino, J., Morin, S., Erbland, J., Grannec, F., Patey, M. D., Vicars, W., Alexander, B.,  
648 Achterberg, E. P., (2013). Isotopic composition of atmospheric nitrate in a tropical marine  
649 boundary layer. *Proceedings of the National Academy of Sciences*, 110(44), 17668–17673.  
650 <https://doi.org/10.1073/pnas.1216639110>  
651

652 Sharma, H. D., Jervis, R. E., & Wong, K. Y. (1970). Isotopic exchange reactions in nitrogen oxides.  
653 *The Journal of Physical Chemistry*, 74(4), 923–933. <https://doi.org/10.1021/j100699a044>  
654

655 Takei, T., Yamazaki, A., Watanabe, T., & Chikazawa, M. (1997). Water adsorption properties on  
656 porous silica glass surface modified by trimethylsilyl groups. *Journal of Colloid and Interface*  
657 *Science*, 188(2), 409–414. <https://doi.org/10.1006/jcis.1997.4777>  
658

659 Urey, H. C. (1947). The thermodynamic properties of isotopic substances. *Journal of the Chemical*  
660 *Society (Resumed)*, 562-581. <https://doi.org/10.1039/JR9470000562>  
661

662 Vicars, W. C., Morin, S., Savarino, J., Wagner, N. L., Erbland, J., Vince, E., Martins, J. M. F.,  
663 Lerner, B. M., Quinn, P. K., Coffman, D. J., Williams, E. J., Brown, S. S., (2013). Spatial and  
664 diurnal variability in reactive nitrogen oxide chemistry as reflected in the isotopic composition of  
665 atmospheric nitrate: Results from the CalNex 2010 field study. *Journal of Geophysical Research:*  
666 *Atmospheres*, 118(18), 10–567. <https://doi.org/10.1002/jgrd.50680>  
667

668 Walters, W. W., & Michalski, G. (2015). Theoretical calculation of nitrogen isotope equilibrium  
669 exchange fractionation factors for various NO<sub>y</sub> molecules. *Geochimica et Cosmochimica Acta*,  
670 164, 284–297. <https://doi.org/10.1016/j.gca.2015.05.029>  
671

672 Walters, W. W., Goodwin, S. R., & Michalski, G. (2015). Nitrogen stable isotope composition  
673 ( $\delta^{15}\text{N}$ ) of vehicle-emitted  $\text{NO}_x$ . *Environmental Science & Technology*, 49(4), 2278–2285.  
674 <https://doi.org/10.1021/es505580v>  
675

676 Walters, W. W., & Michalski, G. (2016). Ab initio study of nitrogen and position-specific oxygen  
677 kinetic isotope effects in the  $\text{NO}+\text{O}_3$  reaction. *The Journal of chemical physics*, 145(22), 224311.  
678 <https://doi.org/10.1063/1.4968562>  
679

680 Walters, W. W., Simonini, D. S., & Michalski, G. (2016). Nitrogen isotope exchange between  $\text{NO}$   
681 and  $\text{NO}_2$  and its implications for  $\delta^{15}\text{N}$  variations in tropospheric  $\text{NO}_x$  and atmospheric nitrate.  
682 *Geophysical Research Letters*, 43(1), 440–448. <https://doi.org/10.1002/2015GL066438>  
683

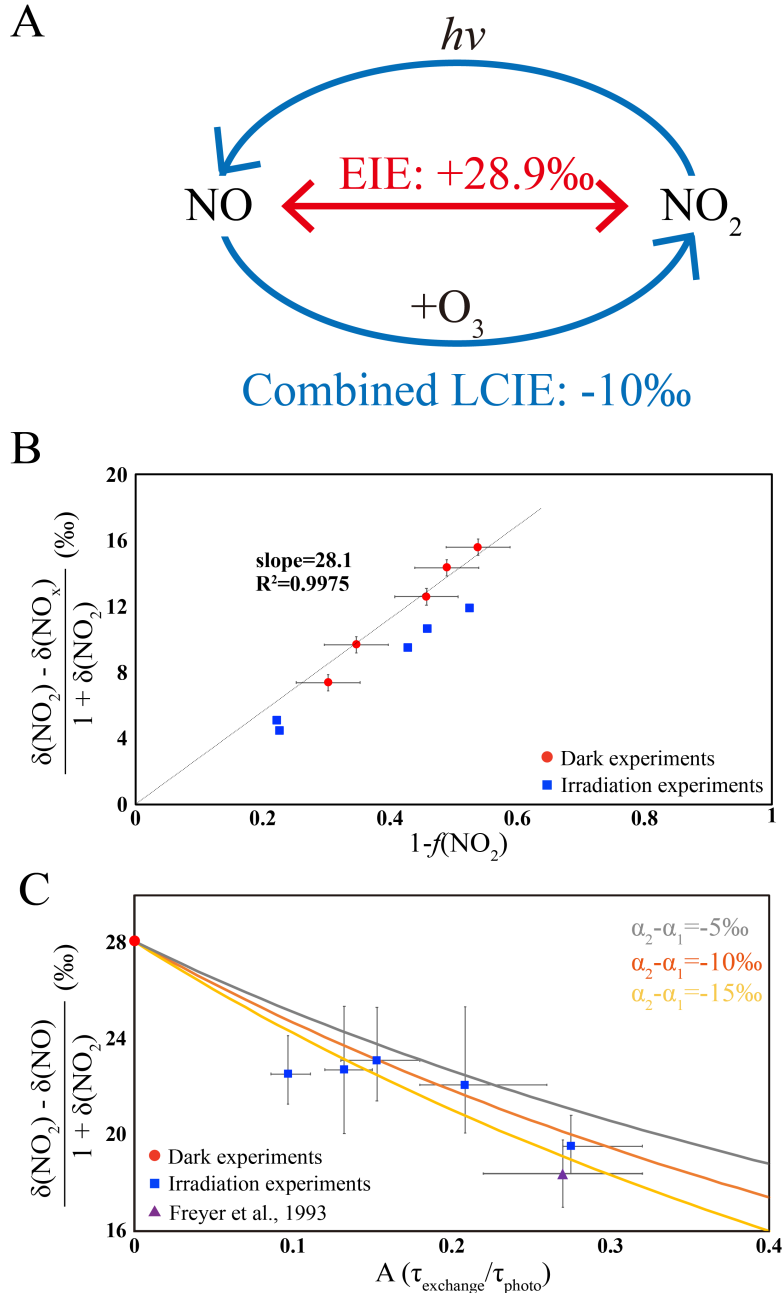
684 Walters, W. W., Fang, H., & Michalski, G. (2018). Summertime diurnal variations in the isotopic  
685 composition of atmospheric nitrogen dioxide at a small midwestern United States city.  
686 *Atmospheric Environment*, 179, 1–11. <https://doi.org/10.1016/j.atmosenv.2018.01.047>  
687

688 Williams, E. L., & Grosjean, D. (1990). Removal of atmospheric oxidants with annular denuders.  
689 *Environmental Science & Technology*, 24(6), 811–814. <https://doi.org/10.1021/es00076a002>  
690

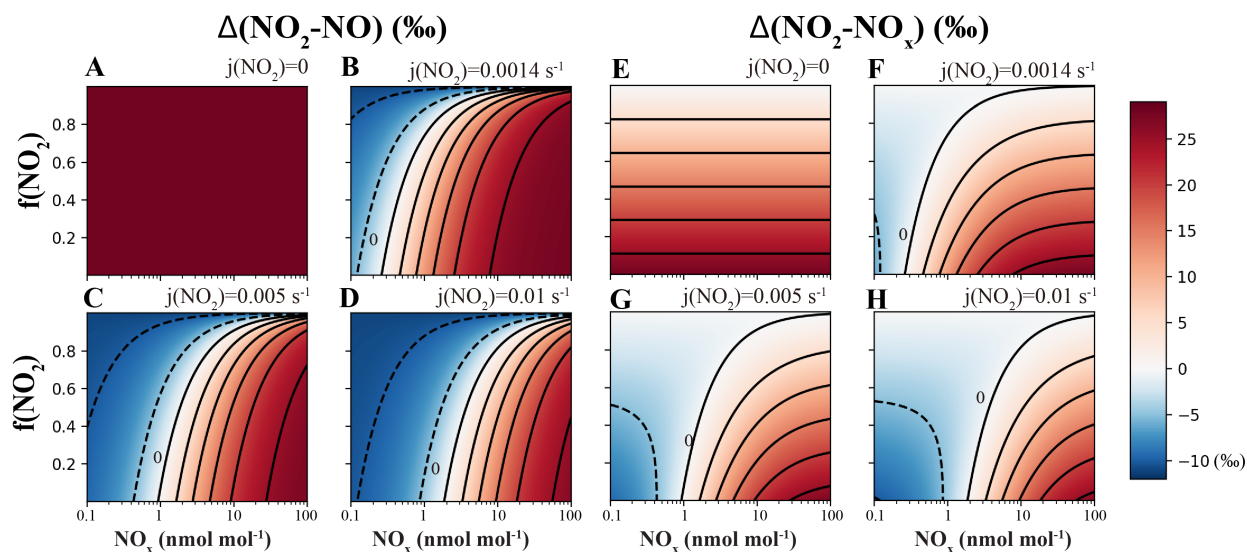
691 Yang, J., Honrath, R. E., Peterson, M. C., Dibb, J. E., Sumner, A. L., Shepson, P. B., Frey, M.,  
692 Jacobi, H.-W., Swanson, A., Blake, N., (2002). Impacts of snowpack emissions on deduced levels  
693 of OH and peroxy radicals at Summit, Greenland. *Atmospheric Environment*, 36(15–16), 2523–  
694 2534. [https://doi.org/10.1016/S1352-2310\(02\)00128-0](https://doi.org/10.1016/S1352-2310(02)00128-0)  
695

696 Zhang, X., Ortega, J., Huang, Y., Shertz, S., Tyndall, G. S., & Orlando, J. J. (2018). A steady-state  
697 continuous flow chamber for the study of daytime and nighttime chemistry under atmospherically  
698 relevant  $\text{NO}$  levels. *Atmospheric Measurement Techniques*, 11(5), 2537–2551.  
699 <https://doi.org/10.5194/amt-11-2537-2018>  
700

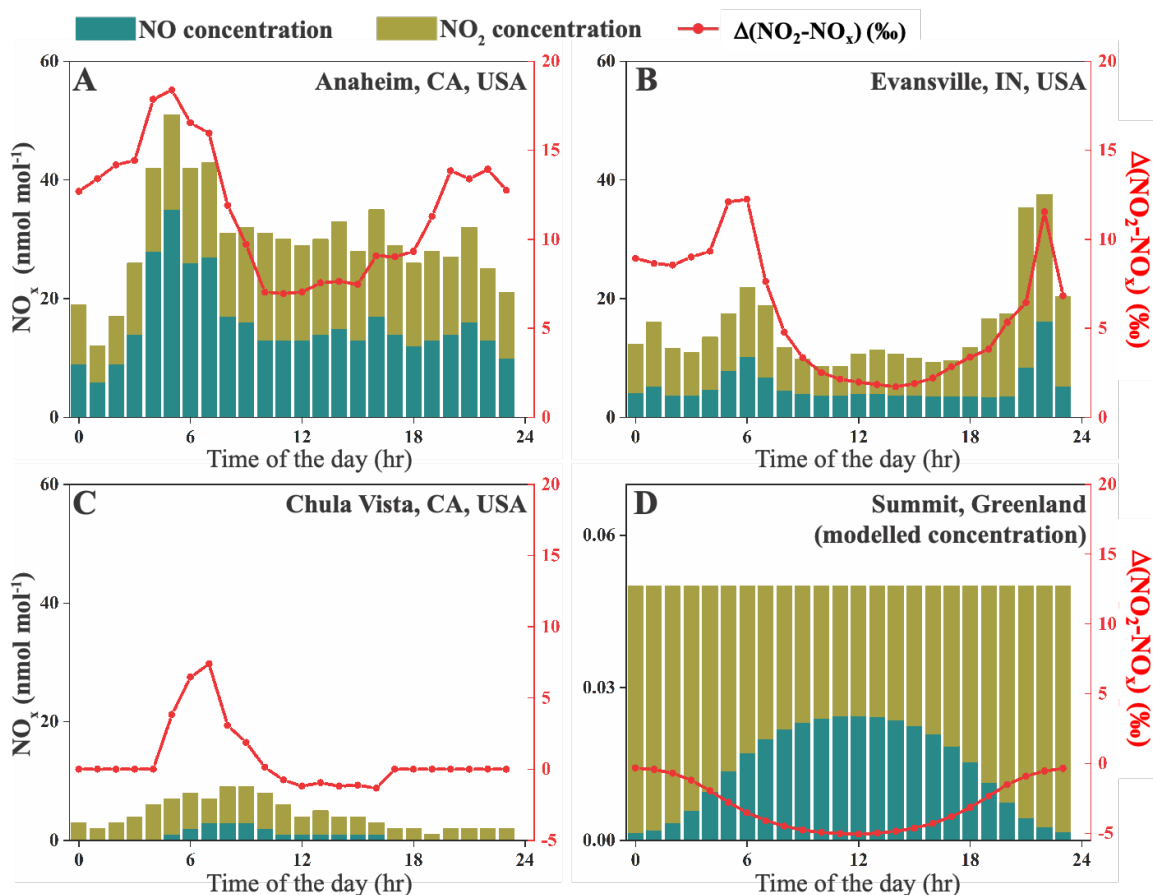
701 Zong, Z., Wang, X., Tian, C., Chen, Y., Fang, Y., Zhang, F., Li, C., Sun, J., Li, J., Zhang, G.,  
702 (2017). First assessment of  $\text{NO}_x$  sources at a regional background site in North China using  
703 isotopic analysis linked with modeling. *Environmental Science & Technology*, 51(11), 5923–5931.  
704 <https://doi.org/10.1021/acs.est.6b06316>



705  
 706 **Fig. 1 A.** a sketch of the isotopic fractionation processes between NO and NO<sub>2</sub>, both fractionation  
 707 factors are determined in this work. **B.** Results from five dark experiments (red circles) yielded a  
 708 line with slope of 28.1‰ and an  $\alpha(\text{NO}_2\text{-NO})$  value of 1.0289, while the results from five UV  
 709 irradiation experiments (blue squares) showed a smaller slope; **C.** Results from five UV irradiation  
 710 experiments (blue squares) and a previous field study (purple triangle), comparing to the dark  
 711 experiments (red circle). The three lines represent different  $(\alpha_2 - \alpha_1)$  values: the  $(\alpha_2 - \alpha_1) = -10\text{‰}$  line  
 712 showed the lowest RMSE to our experimental data as well as the previous field observations. The  
 713 error bars in panels B and C represented the combined uncertainties of NO<sub>x</sub> concentration  
 714 measurements and isotopic analysis.  
 715



716  
 717 **Fig. 2** Calculating isotopic fractionation values between NO-NO<sub>2</sub> ( $\Delta(\text{NO}_2\text{-NO})$ , **A-D**) and NO<sub>x</sub>-  
 718 NO<sub>2</sub> ( $\Delta(\text{NO}_2\text{-NO}_x)$ , **E-H**) at various  $j(\text{NO}_2)$ , NO<sub>x</sub> level and  $f(\text{NO}_2)$  using Eq. (7) and (8). Each  
 719 panel represents a fixed  $j(\text{NO}_2)$  value (showing on the upper right side of each panel), and the  
 720 fractionation values are shown by color. Lines are contours with the same fractionation values, at  
 721 an interval of 5‰, the contour line representing 0‰ was marked on each panel except for A and  
 722 E.



723  
 724 **Fig. 3** NO<sub>x</sub> concentrations and calculated  $\Delta(\text{NO}_2-\text{NO}_x)$  values at four sites. Stacked bars show the  
 725 NO and NO<sub>2</sub> concentrations extracted from monitoring sites (A-C) or calculated using 0-D box  
 726 model (D); the red lines are  $\Delta(\text{NO}_2-\text{NO}_x)$  values at each site. Note that the NO<sub>x</sub> concentration (left-  
 727 y) axis on panel D is different from the rest.  
 728

Experiment	Number	NO conc. (nmol mol <sup>-1</sup> )	NO <sub>2</sub> conc. (nmol mol <sup>-1</sup> )	O <sub>3</sub> conc. (nmol mol <sup>-1</sup> )	δ(NO <sub>2</sub> ) (‰)	f(NO <sub>2</sub> )
Determining δ(NO <sub>x</sub> )	1	0.0	17.8	13.4	-59.5	1.00
	2	0.0	61.3	0.5	-58.9	1.00
	3	0.0	18.9	10.7	-58.0	1.00
Dark experiments	1	16.0	36.8	0.0	-51.8	0.70
	2	33.6	28.8	0.0	-43.9	0.46
	3	6.7	12.6	0.0	-49.6	0.65
	4	16.2	16.9	0.0	-45.1	0.51
	5	20.4	24.2	0.0	-46.8	0.54
Irradiation experiments	1	7.1	6.4	2.8	-47.5	0.47
	2	4.5	5.3	4.5	-48.7	0.54
	3	3.3	4.4	4.2	-49.8	0.57
	4	2.5	8.5	10.7	-54.6	0.77
	5	5.2	18.1	11.0	-54.0	0.78

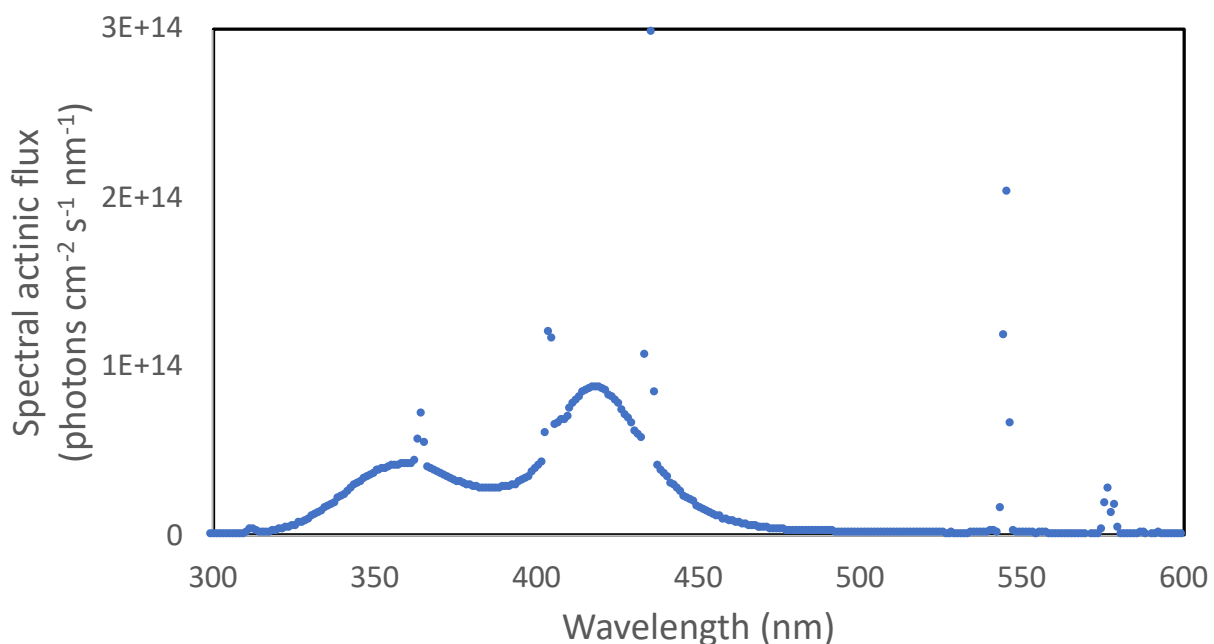
Table 1. Experimental conditions, concentrations of NO, NO<sub>2</sub> and O<sub>3</sub> at steady state, and measured δ(NO<sub>2</sub>) values.

729  
730  
731

732 **Appendix A. Chamber descriptions**

733 The chamber is a 10 m<sup>3</sup> Teflon bag equipped with several standard instruments including  
734 temperature and humidity probe, NO<sub>x</sub> monitor and O<sub>3</sub> monitor. 128 wall-mounted blacklight tubes  
735 surrounded the chamber to mimic tropospheric photochemistry and the photolysis rate of NO<sub>2</sub>  
736 ( $j(\text{NO}_2)$ ) when all lights are on have been previously determined to be  $1.4 \times 10^{-3} \text{ s}^{-1}$ , similar to a  
737  $j(\text{NO}_2)$  coefficient at an 81-degree solar zenith angle. The irradiation spectrum of the blacklights  
738 are shown in Figure A1. The chamber was kept at room temperature and one atmospheric pressure.  
739 Before each experiment, the chamber was flushed with zero air at 40 L min<sup>-1</sup> for at least 12 hours  
740 to ensure the background NO<sub>x</sub>, O<sub>3</sub> and other trace gases were below detection limit.

741



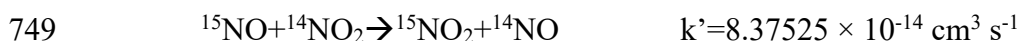
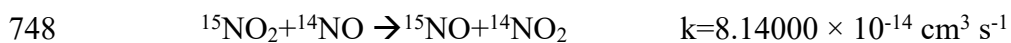
742

743 Figure A1 Spectral actinic flux versus wavelengths of the UV light source used in our experiments.

744

745 **Appendix B. Box model assessing the time needed for NO-NO<sub>2</sub> to reach isotopic equilibrium**

746 The time needed to reach NO-NO<sub>2</sub> isotopic equilibrium during light-off experiments were  
747 assessed using a 0-D box model. This box model contains only two reactions:

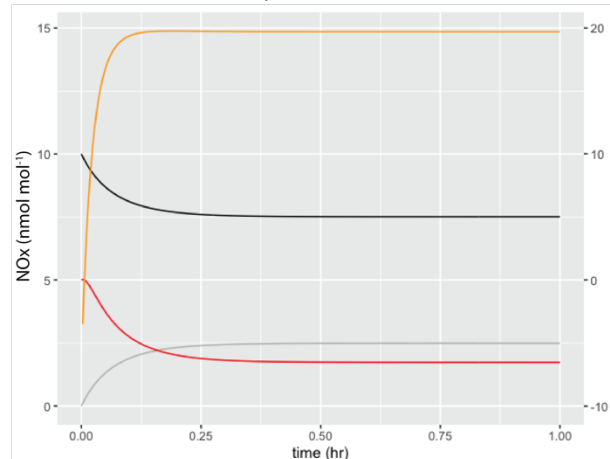


750 Where k and k' are rate constants of the reactions. The differences in rate constants were calculated  
751 by assuming an  $\alpha(\text{NO}_2\text{-NO})$  value of 1.0289. Six simulations were conducted at various initial NO  
752 (with  $\delta^{15}\text{N} = 0\text{‰}$ ) and O<sub>3</sub> levels that were similar to our experiment. Then the  $\delta^{15}\text{N}$  values of NO  
753 and NO<sub>2</sub> during the simulation were calculated from the model and were shown in Figure B1,  
754 suggesting that in our experimental condition, all systems should reach isotopic equilibrium within  
755 1 hr.

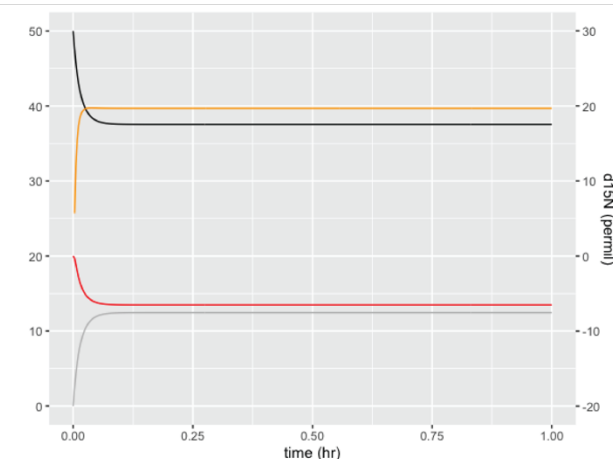
756



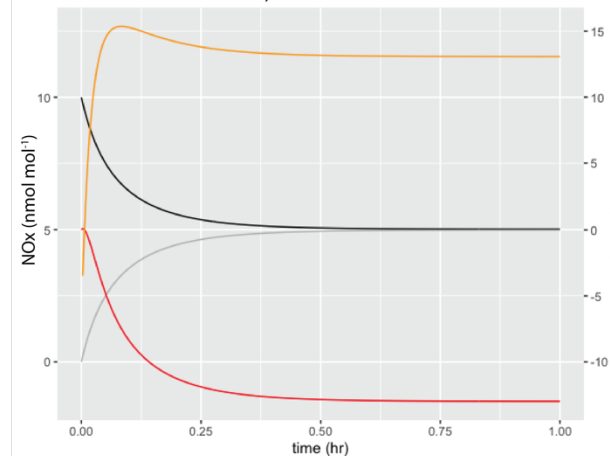
Initial NO=10 nmol mol<sup>-1</sup>, O3=2.5 nmol mol<sup>-1</sup>



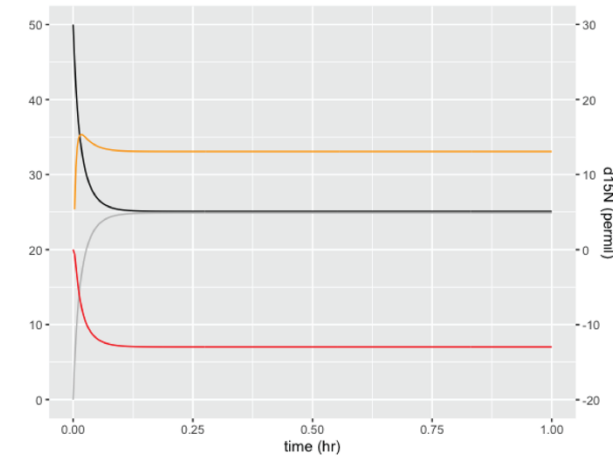
Initial NO=50 nmol mol<sup>-1</sup>, O3=12.5 nmol mol<sup>-1</sup>



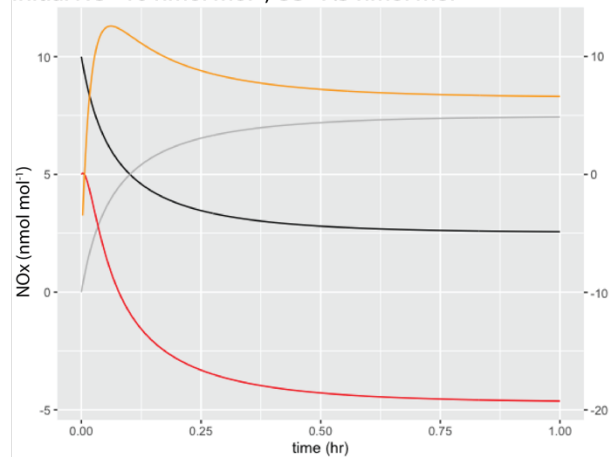
Initial NO=10 nmol mol<sup>-1</sup>, O3=5 nmol mol<sup>-1</sup>



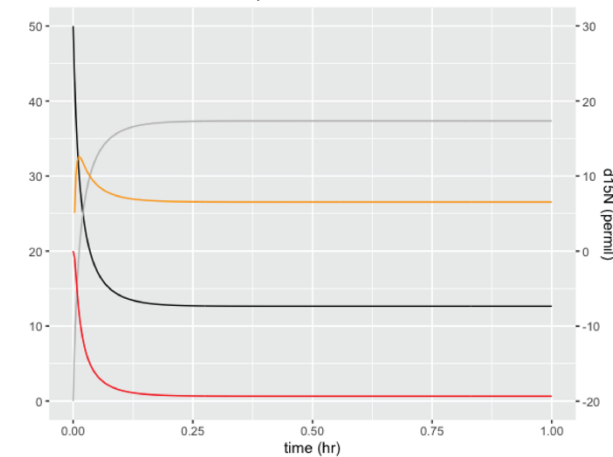
Initial NO=50 nmol mol<sup>-1</sup>, O3=25 nmol mol<sup>-1</sup>



Initial NO=10 nmol mol<sup>-1</sup>, O3=7.5 nmol mol<sup>-1</sup>



Initial NO=50 nmol mol<sup>-1</sup>, O3=37.5 nmol mol<sup>-1</sup>



757 ——— NO concentration ——— NO<sub>2</sub> concentration ——— δ(NO<sub>2</sub>) ——— δ(NO)

758 Figure B1 Simulated NO-NO<sub>2</sub> isotopic equilibrium process in the chamber at various NO and O<sub>3</sub>  
759 concentrations.

760 **Appendix C. Deriving Equations 7 and 8**

761 When the system (R1-R6) reaches steady-state, we have:

762 
$$d[^{15}\text{NO}_2]/dt=0 \quad \text{Eq. (C1)}$$

763 Therefore, using R1-R6:

764 
$$k_1 [^{15}\text{NO}_2][^{14}\text{NO}] + j(\text{NO}_2)\alpha_1 [^{15}\text{NO}_2] =$$

765 
$$k_5\alpha_2 [^{15}\text{NO}][\text{O}_3] + k_1\alpha(\text{NO}_2-\text{NO}) [^{15}\text{NO}][^{14}\text{NO}_2] \quad \text{Eq. (C2)}$$

766 From here we refer  $^{14}\text{NO}_2$  and  $^{14}\text{NO}$  as  $\text{NO}_2$  and  $\text{NO}$  for convenience, rearrange the above equation,  
767 we get:

768 
$$\frac{[^{15}\text{NO}_2]}{[^{15}\text{NO}]} = \frac{k_5\alpha_2[\text{O}_3] + k_1\alpha(\text{NO}_2-\text{NO}) [\text{NO}_2]}{j_{\text{NO}_2}\alpha_1 + k_1[\text{NO}]} \quad \text{Eq. (C3)}$$

769 Meantime, since the Leighton cycle reaction still holds for the majority isotopes ( $\text{NO}$  and  $\text{NO}_2$ ),  
770 we have:

771 
$$j_{\text{NO}_2}[\text{NO}_2] = k_5[\text{NO}][\text{O}_3] \quad \text{Eq. (C4)}$$

772 Thus,

773 
$$\frac{[\text{NO}_2]}{[\text{NO}]} = \frac{k_5 \times [\text{O}_3]}{j_{\text{NO}_2}} \quad \text{Eq. (C5)}$$

774 From the text, when  $j_{\text{NO}_2} > 0$ , we defined  $A = \tau_{\text{exchange}}/\tau_{\text{photo}} = j_{\text{NO}_2}/(k_1 \times [\text{NO}])$ . Using the above  
775 equations, we know:

776 
$$\frac{j_{\text{NO}_2}}{[\text{NO}]} = \frac{k_5[\text{O}_3]}{[\text{NO}_2]} = Ak_1 \quad \text{Eq. (C6)}$$

777 
$$\frac{j_{\text{NO}_2}}{k_1[\text{NO}]} = \frac{k_5[\text{O}_3]}{k_1[\text{NO}_2]} = A \quad \text{Eq. (C7)}$$

778 Next, to calculate  $\delta(\text{NO}_2) - \delta(\text{NO})$ , we use the definition of delta notation:

779 
$$\delta(\text{NO}_2) - \delta(\text{NO}) = R_{\text{NO}_2}/R_{\text{std}} - R_{\text{NO}}/R_{\text{std}} = (R_{\text{NO}_2}/R_{\text{NO}} - 1)(1 + \delta(\text{NO})) \quad \text{Eq. (C8)}$$

780

781 
$$\frac{R_{NO_2}}{R_{NO}} = \frac{[^{15}NO_2][NO]}{[^{15}NO][NO_2]} = \frac{k_5\alpha_2[O_3][NO]+k_1\alpha(NO_2-NO)[NO_2][NO]}{j_{NO_2}\alpha_1[NO_2]+k_1[NO][NO_2]} \quad \text{Eq. (C9)}$$

782 Divide both side by  $k_1[NO][NO_2]$ :

783 
$$\frac{R_{NO_2}}{R_{NO}} = \frac{\frac{k_5\alpha_2[O_3]}{k_1[NO_2]}+\alpha(NO_2-NO)}{\frac{j_{NO_2}\alpha_1}{k_1[NO]}+1} \quad \text{Eq. (C10)}$$

784 Rearrange and substitute  $\frac{k_5[O_3]}{k_1[NO_2]}$  and  $\frac{j_{NO_2}}{k_1[NO]}$  with A:

785 
$$\frac{R_{NO_2}}{R_{NO}} = \frac{\alpha_2A+\alpha(NO_2-NO)}{\alpha_1A+1} \quad \text{Eq. (C11)}$$

786 
$$\frac{R_{NO}}{R_{NO_2}} = \frac{\alpha_1A+1}{\alpha_2A+\alpha(NO_2-NO)} \quad \text{Eq. (C12)}$$

787 
$$\frac{R_{NO}}{R_{NO_2}} - 1 = \frac{(\alpha_1-\alpha_2)A-(\alpha(NO_2-NO)-1)}{\alpha_1A+\alpha(NO_2-NO)} \quad \text{Eq. (C13)}$$

788 Thus,

789 
$$\delta(NO_2)-\delta(NO)=\frac{(\alpha_2-\alpha_1)A+(\alpha(NO_2-NO)-1)}{\alpha_1A+\alpha(NO_2-NO)}(1+\delta(NO_2)) \quad \text{Eq. (C14)}$$

790 Then, using mass balance:

791 
$$\delta(NO_2)f(NO_2)+\delta(NO)(1-f(NO_2)) = \delta(NO_x) \quad \text{Eq. (C15)}$$

792 We can derive Eq. 8:

793 
$$\delta(NO_2)-\delta(NO_x)=\frac{(\alpha_2-\alpha_1)\times A+(\alpha(NO_2-NO)-1)}{\alpha_1A+\alpha(NO_2-NO)}(1+\delta(NO_2))(1-f(NO_2)) \quad \text{Eq. (C16)}$$